

Axion-like particles explain the unphysical redshift-dependence of AGN gamma-ray spectra

Giorgio Galanti*

*Dipartimento di Fisica, Università dell'Insubria,
Via Valleggio 11, I - 22100 Como, Italy*

Marco Roncadelli†

INFN, Sezione di Pavia, Via A. Bassi 6, I - 27100 Pavia, Italy

Alessandro De Angelis‡

INFN, Sezione di Padova, Via Marzolo 8, I - 35131 Padova, Italy

Giovanni F. Bignami§

INAF, Viale del parco Mellini 84, I - 00136 Roma, Italy

Blazars are a class of Active Galactic Nuclei (AGN) known to be powerful very-high-energy (VHE, 100 GeV – 100 TeV) celestial gamma-ray emitters. At the time of writing, 41 blazars, spread all over the sky and with known redshift in the range $0.0215 \leq z \leq 0.635$, have been observed in the VHE band by the Imaging Atmospheric Cherenkov Telescopes H.E.S.S., MAGIC and VERITAS. Thus, they represent an isotropic and relatively local extragalactic sample, unaffected by significant cosmological evolution. The blazar emitted spectra are well fitted by a power law with index Γ_{em} . We show that the Γ_{em} distribution exhibits an unexpected and previously unnoticed unphysical redshift-dependence. We demonstrate that this result is not due to any selection effect. It is difficult to imagine an intrinsic mechanism which could lead to such a spectral variation, and so this result seriously challenges the conventional view. We propose that such a behavior is explained by oscillations between the VHE gamma-rays and Axion-Like Particles (ALPs), taking place in extragalactic magnetic fields. We recall that ALPs are predicted by several extensions of the Standard Model and especially by those based on superstring theories. Moreover, they are attracting growing interest being also good candidates for cold dark matter. As a consequence of the photon-ALP oscillation mechanism, the Γ_{em} distribution becomes *redshift-independent*, indeed in agreement with the physical expectation. This is a highly nontrivial fact, which therefore provides a preliminary evidence for the existence of ALPs. Thus, besides physics laboratory data, astrophysical VHE data from e.g. the upcoming CTA (Cherenkov Telescope Array) can settle this issue. Our Universe may in this way be offering us a compelling reason to push physics beyond the Standard Model along a very specific direction, which possibly sheds light also on the nature of cold dark matter.

PACS numbers: 14.80.Mz, 95.30.-k, 95.85.Pw, 95.85.Ry, 98.70.Rz, 98.70.Vc, 98.70.Sa

*Electronic address: gam.galanti@gmail.com

†Electronic address: marco.roncadelli@pv.infn.it

‡Electronic address: deangelis.alessandro@gmail.com

§Electronic address: giovanni.bignami@gmail.com

I. INTRODUCTION

Owing to observations performed with the Imaging Atmospheric Cherenkov Telescopes (IACTs) like H.E.S.S. [1], MAGIC [2] and VERITAS [3], at the time of writing 41 blazars with known redshift have been detected in the very-high-energy (VHE) range (100 GeV – 100 TeV) [4].

It turns out that all their observed spectra are well fitted by a single power-law, and so they have the form $\Phi_{\text{obs}}(E_0, z) = K_{\text{obs}}(z) E_0^{-\Gamma_{\text{obs}}(z)}$, where E_0 is the observed energy while $K_{\text{obs}}(z)$ and $\Gamma_{\text{obs}}(z)$ denote a constant and the observed spectral index, respectively, for a source at redshift z .

Unfortunately, the observational results do not provide any *direct* information about the intrinsic properties of the sources, as the gamma-ray data strongly depend on the nature of photon propagation. Indeed, according to conventional physics the blazar spectra in the VHE range are strongly affected by the presence of the Extragalactic Background Light (EBL), namely the infrared/optical/ultraviolet background photons emitted by all galaxies since their birth [5]. However, it should be kept in mind that if some yet-to-be-discovered new physics changes the photon propagation, then some intrinsic source properties that are currently believed to be true may actually be incorrect.

Another piece of information that we need is that the two competing models for VHE blazar emission – namely the Synchro-Self-Compton (SSC) mechanism [6, 7] and the Hadronic Pion Production (HPP) in proton-proton scattering [8] – both predict emitted spectra which, to a good approximation, have a single power-law behavior $\Phi_{\text{em}}(E) = K_{\text{em}} E^{-\Gamma_{\text{em}}}$ for all the presently observed VHE blazars.

The relation between $\Phi_{\text{obs}}(E_0, z)$ and $\Phi_{\text{em}}(E)$ can be expressed in general terms as

$$\Phi_{\text{obs}}(E_0, z) = P_{\gamma \rightarrow \gamma}(E_0, z) \Phi_{\text{em}}(E_0(1+z)) , \quad (1)$$

where $P_{\gamma \rightarrow \gamma}(E_0, z)$ is the photon survival probability from the source to us, and is usually written in terms of the optical depth $\tau_{\gamma}(E_0, z)$ as

$$P_{\gamma \rightarrow \gamma}(E_0, z) = e^{-\tau_{\gamma}(E_0, z)} . \quad (2)$$

In this paper we are concerned with the possible correlation between the blazar *emitted spectra* and their *redshift*.

We are now in position to outline the structure of the paper. In Section II we report all observational information needed for the present analysis. Section III is devoted to inferring for any source the emitted spectral index – to be denoted by $\Gamma_{\text{em}}^{\text{CP}}(z)$ – starting from the observed one $\Gamma_{\text{obs}}(z)$ assuming conventional physics, namely taking into account the effect of the EBL absorption alone. We next plot the values of $\Gamma_{\text{em}}^{\text{CP}}(z)$ as a function of redshift z for all sources. After performing a statistical analysis of this result, we end up with the conclusion that the best-fit regression line of the spectral index distribution decreases as the redshift increases. *A priori*, this behavior might be explained as a selection effect. Yet, a deeper scrutiny based on observational information shows that this is by no means the case, leading in fact to the conclusion that it is unphysical. This finding therefore poses a serious challenge to the conventional view. In Section IV we identify the key-requirements that an *ideal scenario* should satisfy in order for the best-fit regression line of the spectral index distribution to exhibit a physically satisfactory behavior. In Section V we investigate whether such an ideal scenario can be implemented within conventional physics, but our conclusion is negative. As an attempt to correct such a drawback, in Section VI we introduce Axion-Like Particles (ALP) [9]. They are spin-zero, neutral and extremely light pseudo-scalar bosons predicted by several extensions of the Standard Model of particle physics, and especially by those based on superstring theories [10–19]. Depending on their mass and two-photon coupling, they can be quite good candidates for cold dark matter [20] and give rise to

very interesting astrophysical effects (to be discussed in Section VII), so that nowadays ALPs are attracting growing interest. Specifically, we suppose that photon-ALP oscillations take place in the extragalactic magnetic fields, as first proposed in [21]. As a consequence, photon propagation gets affected by EBL as well as by photon-ALP oscillations, whose combined effect is to *substantially reduce* the cosmic opacity brought about by the EBL alone. Accordingly, we re-derive for every source the emitted spectral index – to be denoted by $\Gamma_{\text{em}}^{\text{ALP}}(z)$ – starting from the observed one $\Gamma_{\text{obs}}(z)$. Proceeding then as before, we plot again the values of $\Gamma_{\text{em}}^{\text{ALP}}(z)$ as a function of redshift z for all sources. A statistical analysis of this result shows that now the best-fit regression line of the spectral index distribution becomes *independent* of redshift. Moreover, the values of $\Gamma_{\text{em}}^{\text{ALP}}(z)$ for the individual blazars exhibit a small scatter about such a best-fit regression line. Actually, our ideal scenario turns out to be fully implemented within the present context. We stress that the fact that the best-fit regression line turns out to be a straight line horizontal in the $\Gamma_{\text{em}}^{\text{ALP}} - z$ plane is a highly nontrivial circumstance, which is in agreement with the physical expectation and provides a strong hint of the existence of ALPs. Finally, in Section VII we briefly discuss the new view emerging from our result, its relevance – also in connection with other VHE astrophysical achievements employing ALPs – and its implications for the future of VHE astrophysics. In order to avoid breaking the main line of thought by somewhat involved technicalities concerning the evaluation of the photon survival probability in the presence of ALPs, we report this matter in the Appendix.

II. OBSERVATIONAL INFORMATION

The observational quantities concerning every blazar which are relevant for the present analysis are: the redshift z , the observed spectral index $\Gamma_{\text{obs}}(z)$ with the associated error bar and the energy range ΔE_0 where the source is observed. They are summarized in Table III, and the observed spectral indexes are plotted in Fig. 1 as a function of the redshift for all VHE sources detected at the time of writing.

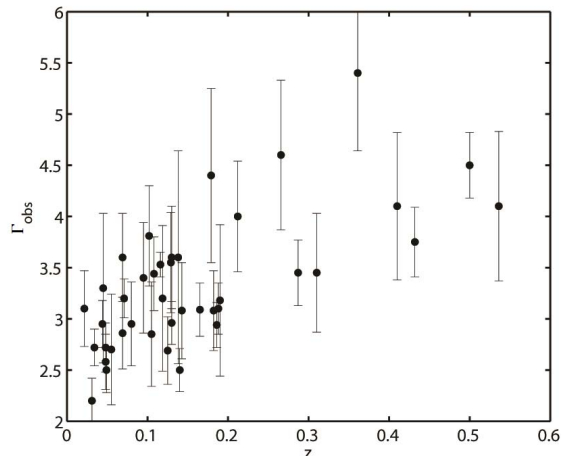


FIG. 1: The observed values of the spectral index $\Gamma_{\text{obs}}(z)$ are plotted versus the source redshift z for all blazars detected at the time of writing in the VHE band as given in Table III, from which the observational error bars are also taken.

Moreover, in order to clarify a situation that we shall encounter, we will also need two further quantities. One is the observed flux normalization constant $K_{\text{obs}}(z)$ entering the expression of

$\Phi_{\text{obs}}(E_0, z)$. Clearly, for the sake of comparison among the values of $K_{\text{obs}}(z)$ for all sources we have normalized all spectra in such a way that $K_{\text{obs}}(z)$ always coincides with the nominal observed flux at the fiducial energy $E_* = 300 \text{ GeV}$. This convention is implicitly assumed henceforth throughout the paper, and so all energies will be expressed in the unit of $E_* = 300 \text{ GeV}$. The other quantity is the observed flux inside ΔE_0 , to be denoted by $F_{\text{obs}, \Delta E_0}(z)$. For our needs the associated error bars are irrelevant. They are both plotted in Fig. 2 as a function of the redshift for all considered VHE sources.

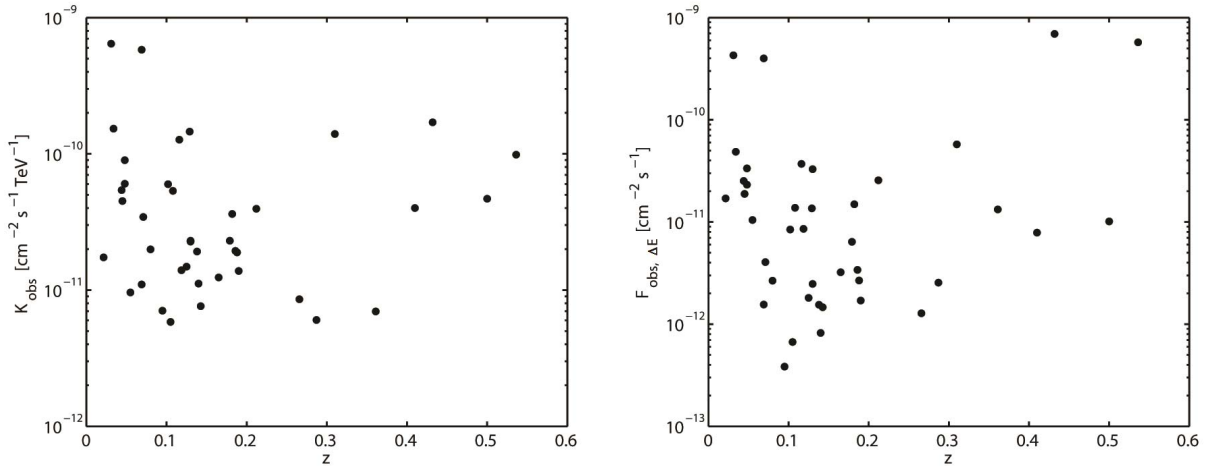


FIG. 2: Observed flux normalization constant $K_{\text{obs}}(z)$ and observed flux $F_{\text{obs}, \Delta E_0}(z)$ inside ΔE_0 . *Left panel:* The values of $K_{\text{obs}}(z)$ are plotted versus the source redshift z for all blazars detected at the time of writing in the VHE band as given in Table III. *Right panel:* The values of $F_{\text{obs}, \Delta E_0}(z)$ are plotted versus the source redshift z for all blazars considered in the left panel.

III. CONVENTIONAL PROPAGATION IN EXTRAGALACTIC SPACE

After a long period of uncertainty on the EBL precise spectral energy distribution and photon number density, today a convergence seems to be reached [5], well represented e.g. by the model of Franceschini, Rodighiero and Vaccari (FRV) [22], which we use for convenience.

Owing to $\gamma\gamma \rightarrow e^+e^-$ scattering off EBL photons [23, 24], the emitted VHE blazar photons undergo an energy-dependent absorption, so that the VHE photon survival probability is given by Eq. (2) with $\tau_\gamma(E_0, z) \rightarrow \tau_\gamma^{\text{FRV}}(E_0, z)$, where $\tau_\gamma^{\text{FRV}}(E_0, z)$ is the optical depth of the EBL as evaluated within the FRV model in a standard fashion using the photon spectral number density [25–27]. As a consequence, the observed flux $\Phi_{\text{obs}}(E_0, z)$ is related to the emitted one $\Phi_{\text{em}}(E)$ by

$$\Phi_{\text{obs}}(E_0, z) = e^{-\tau_\gamma^{\text{FRV}}(E_0, z)} \Phi_{\text{em}}(E_0(1+z)). \quad (3)$$

Let us begin by deriving the emitted spectrum of every source, starting from the observed one, within conventional physics. As a preliminary step, we rewrite Eq. (3) as

$$\Phi_{\text{em}}(E_0(1+z)) = e^{\tau_\gamma^{\text{FRV}}(E_0, z)} K_{\text{obs}}(z) E_0^{-\Gamma_{\text{obs}}(z)}. \quad (4)$$

Owing to the presence of the exponential in the r.h.s. of Eq. (4), $\Phi_{\text{em}}(E_0(1+z))$ cannot behave as an exact power law (unless $\tau_\gamma^{\text{FRV}}(E_0, z)$ has a logarithmic z -dependence). Yet, we have pointed

out that it is expected to be close to it. So, we best-fit $\Phi_{\text{em}}(E_0(1+z))$ to a single power-law with spectral index $\Gamma_{\text{em}}^{\text{CP}}(z)$ – namely to $K_{\text{em}}^{\text{CP}}(z) [(1+z)E_0]^{-\Gamma_{\text{em}}^{\text{CP}}(z)}$ – over the energy range ΔE_0 where the source is observed. Incidentally, we neglect error bars in the values of $\tau_{\gamma}^{\text{FRV}}(E_0, z)$ because they are not quoted by FRV. Since $\Gamma_{\text{em}}^{\text{CP}}(z)$ depends linearly on $\Gamma_{\text{obs}}(z)$, the inferred values of $\Gamma_{\text{em}}^{\text{CP}}(z)$ have the same error bars as the values of $\Gamma_{\text{obs}}(z)$ reported in Table III. We plot the values of $\Gamma_{\text{em}}^{\text{CP}}(z)$ versus the source redshift z for all our blazars in the left panel of Fig. 3. Of course, we are well aware that the best procedure would be to de-absorb each point of the observed spectrum, thereby getting the emitted spectrum and next applying to it the above best-fitting procedure. Unfortunately, such a strategy is not viable in practice because the single observed energy points with related error bars are not available from published papers. Nevertheless, the difference between the two procedures can be relevant only for those sources whose highest energy points are affected by a large uncertainty, like 1ES 0229+200 which is observed up to about 11 TeV.

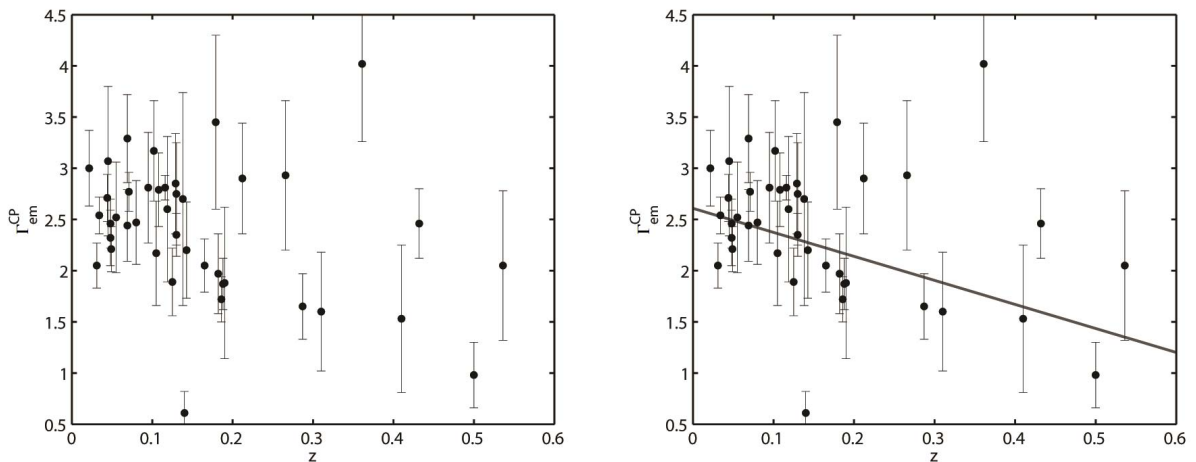


FIG. 3: Emitted spectral index and best-fit regression line in conventional physics. *Left panel:* The values of $\Gamma_{\text{em}}^{\text{CP}}(z)$ are plotted versus the source redshift z for all blazars detected at the time of writing in the VHE band with the corresponding error bars. *Right panel:* Same as left panel, but with superimposed the best-fit straight regression line with $\chi_{\text{red}}^2 = 3.49$.

We proceed by performing a statistical analysis of all values of $\Gamma_{\text{em}}^{\text{CP}}(z)$ as a function of z . Specifically, we use the least square method and try to fit the data with one parameter (horizontal straight line), two parameters (first-order polynomial), and three parameters (second-order polynomial). In order to test the statistical significance of the fits we evaluate the corresponding χ_{red}^2 . The values of the χ_{red}^2 obtained for the three fits are 4.03, 3.49 and 3.56, respectively. Thus, data appear to be best-fitted by the first-order polynomial $\Gamma_{\text{em}}^{\text{CP}}(z) = 2.61 - 2.35 z$. The distribution of $\Gamma_{\text{em}}^{\text{CP}}(z)$ as a function of z with the best-fit straight regression line as defined by the last equation is plotted in the right panel of Fig. 3.

Because the BL Lac 1ES 0229+200 has such an anomalously hard spectrum – as it is evident from the left panel of Fig. 3 – it is worthwhile to check the robustness of our conclusion by repeating the same statistical exercise *without* that source. In this case, we find $\chi_{\text{red}}^2 = 2.35$, $\chi_{\text{red}}^2 = 1.83$ and $\chi_{\text{red}}^2 = 1.87$ for the three above fits, and so now data are best-fitted by the first-order polynomial $\Gamma_{\text{em}}^{\text{CP}}(z) = 2.68 - 2.21 z$. Obviously, the quality of the fit is strongly improved, but the previous result is basically unchanged.

Clearly, the best-fit straight regression line in the right panel of Fig. 3 implies that blazars with harder spectra are found *only* at larger redshift. What is the *physical meaning* of this fact?

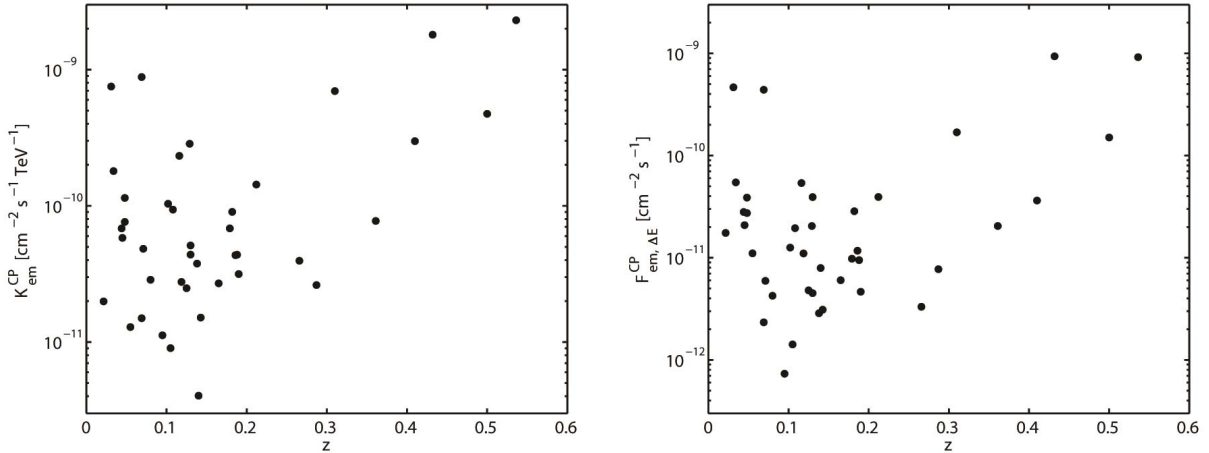


FIG. 4: Emitted flux normalization constant $K_{\text{em}}^{\text{CP}}(z)$ and emitted flux $F_{\text{em},\Delta E}^{\text{CP}}(z)$ inside ΔE in conventional physics. *Left panel:* The emitted values of $K_{\text{em}}^{\text{CP}}(z)$ are plotted versus the source redshift z for all blazars detected at the time of writing in the VHE band as given in Table III. *Right panel:* The values of $F_{\text{em},\Delta E}^{\text{CP}}(z)$ are plotted versus the source redshift z for all blazars considered in the left panel.

Since we are concerned with a relatively local sample, cosmological evolutionary effects are insignificant. Moreover, we have to address all possible selection biases.

- As we look at larger distances only the brighter sources are observed while the fainter ones progressively disappear.
- Looking at greater distances entails that larger regions of space are probed, and so – under the assumption of an uniform source distribution – a larger number of brighter blazars should be detected. Let us denote by $F_{\text{em},\Delta E}^{\text{CP}}(z)$ the emitted flux of each source inside $\Delta E = (1+z)\Delta E_0$. Now, the physical explanation of the best-fit straight regression line in the right panel of Fig. 3 would naturally arise provided that $F_{\text{em},\Delta E}^{\text{CP}}(z)$ *tightly correlates* with $\Gamma_{\text{em}}^{\text{CP}}(z)$ in such a way that *brighter sources have harder spectra*. Then the above selection bias translates into the statement that looking at greater distances implies that a larger number of blazars with harder spectra should be observed, which is just what the right panel of Fig. 3 tells us. So, the real question concerns the existence of a tight correlation between $F_{\text{em},\Delta E}^{\text{CP}}(z)$ and $\Gamma_{\text{em}}^{\text{CP}}(z)$.
- Similarly, a logically consistent possibility would be that the jet opening angle δ were *tightly correlated* to $\Gamma_{\text{em}}^{\text{CP}}(z)$ so that sources with stronger beaming had harder spectra: in such a situation – under the previous assumption of an uniform source distribution – the probability that the beam points towards us increases as larger regions of space are probed, and so sources with harder spectra would be more copiously found at larger distances, again in agreement with what the right panel of Fig. 3 entails.

In order to get a deeper insight into these issues, we plot the values of the emitted flux normalization constant $K_{\text{em}}^{\text{CP}}(z)$ versus the source redshift for all our blazars in the left panel of Fig. 4, while the values of $F_{\text{em},\Delta E}^{\text{CP}}(z)$ are similarly plotted in the right panel of Fig. 4. A first look at the right panel of Fig. 4 shows that the first two expected selection biases are in fact present, thereby providing a check of our procedure. Yet, a much more interesting information comes by comparing

the two panels of Fig. 4. Indeed, we see that a *tight correlation* instead exists between $F_{\text{em},\Delta E}^{\text{CP}}(z)$ and $K_{\text{em}}^{\text{CP}}(z)$, especially at large distances: the patterns of the points representing the same source in both panels have nearly the same shape, especially for $z > 0.3$. This fact implies that $F_{\text{em},\Delta E}^{\text{CP}}(z)$ and $\Gamma_{\text{em}}^{\text{CP}}(z)$ can only be *loosely correlated*, otherwise the tight correlation between $F_{\text{em},\Delta E}^{\text{CP}}(z)$ and $K_{\text{em}}^{\text{CP}}(z)$ would be upset. In addition, the brightest blazars are present at *any* redshift. Finally, a glance at both the right panel of Fig. 4 and the left panel of Fig. 3 shows that the brightest blazars lying at $z < 0.3$ turn out to have *soft* spectra. As a consequence, the cheap explanation outlined in the second item concerning the behavior of the best-fit straight regression line in the right panel of Fig. 3 is doomed to failure. Clearly, the same argument applies equally well if we suppose that δ tightly correlates with $\Gamma_{\text{em}}^{\text{CP}}(z)$ as assumed in the third item, because otherwise the tight correlation between $F_{\text{em},\Delta E}^{\text{CP}}(z)$ and $K_{\text{em}}^{\text{CP}}(z)$ would again be destroyed. Actually, the present issue can be directly settled very easily by comparing the values of $\Gamma_{\text{em}}^{\text{CP}}(z)$ reported in Table IV with those estimated for δ in [28]. What is found is that no correlation whatsoever between $\Gamma_{\text{em}}^{\text{CP}}(z)$ and δ exists.

It is difficult to imagine an intrinsic mechanism which could explain the considered best-fit straight regression line in a physically satisfactory way within conventional physics. We are therefore led to regard the situation emerging from the above discussion as manifestly unphysical, and these surprisingly and previously unnoticed results seriously challenge the conventional view.

IV. AN IDEAL SCENARIO

Sic stantibus rebus, we are naturally led to ponder which kind of ideal scenario could explain our findings, without asking at this stage which sort of new physics allows for the possibility of its accomplishment. Our conclusion is that the distribution of the values of $\Gamma_{\text{em}}(z)$ for all considered blazars should enjoy two properties.

- Assuming that the tight correlation between $F_{\text{em},\Delta E}(z)$ and $K_{\text{em}}(z)$ found above in conventional physics persists in our ideal scenario, then the best-fit regression line of the distribution of the values of $\Gamma_{\text{em}}(z)$ versus the source redshifts should be very close to straight and horizontal.
- Almost all the values of $\Gamma_{\text{em}}(z)$ – say, 95 % of them – should lie inside a rather thin strip about the nearly horizontal best-fit straight regression line.

Let us explain why. Obviously we have by definition that $F_{\text{em},\Delta E}(z)$ must depend on both $K_{\text{em}}(z)$ and $\Gamma_{\text{em}}(z)$, which means that the functional relation $F_{\text{em},\Delta E}(z) = \mathcal{F}(K_{\text{em}}(z), \Gamma_{\text{em}}(z))$ should hold true. Still, in order for a tight correlation between $F_{\text{em},\Delta E}(z)$ and $K_{\text{em}}(z)$ to show up $\Gamma_{\text{em}}(z)$ should be nearly independent of z . Manifestly, in order for this to be the case the two above conditions should be met. Accordingly, the values of $\Gamma_{\text{em}}(z)$ would be in the same ballpark regardless of the redshift, so that the presence of sources with harder spectra only at larger redshifts would be avoided. Moreover, our ideal scenario is in agreement with the absence of cosmologically evolutionary effects (note that we have dropped the symbol CP in all quantities, since we do not know at this stage whether the considered scenario can be implemented within conventional physics).

V. AN ATTEMPT BASED ON CONVENTIONAL PHYSICS

In line with the conclusions of Section IV, we pursue the alternative strategy of best-fitting the same data set considered before with a horizontal straight line, which turns out to be $\Gamma_{\text{em}}^{\text{CP}}(z) = 2.32$.

However, this strategy does not work. In the first place, now we have $\chi_{\text{red}}^2 = 4.03$, which seems unduly large. Furthermore, if we want to encompass 95 % of the observed sources, we have to allow for a spread $\Delta\Gamma_{\text{em}}^{\text{CP}} = 0.95$ both above and below the horizontal fitting straight line. The value of the total spread then amounts to 82 % of the one-parameter fitting value 2.32. This is shown in Fig. 5. Manifestly, the resulting scatter in the values of $\Gamma_{\text{em}}^{\text{CP}}(z)$ is large and would destroy the tight correlation between $F_{\text{em},\Delta E}^{\text{CP}}(z)$ and $K_{\text{em}}^{\text{CP}}(z)$. Thus, we conclude that our ideal scenario conflicts with conventional physics, and so the addressed problem remains unsolved, thereby exacerbating the above shortcoming of the conventional view.

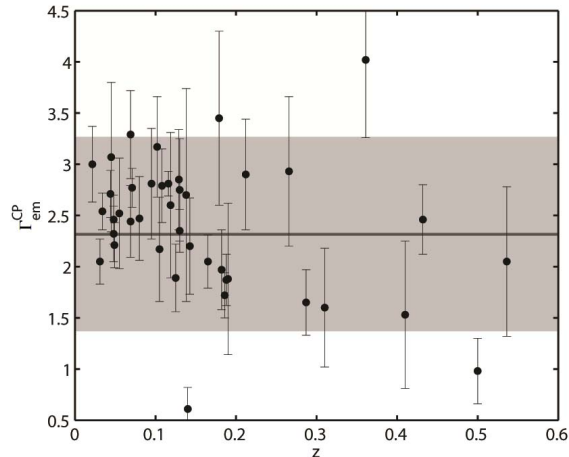


FIG. 5: Horizontal fitting straight line in conventional physics. The values of $\Gamma_{\text{em}}^{\text{CP}}(z)$ are plotted versus the source redshift z for all blazars detected at the time of writing in the VHE band with the corresponding error bars. Superimposed is a horizontal fitting straight line with $\chi_{\text{red}}^2 = 4.03$ and $\Gamma_{\text{em}}^{\text{CP}}(z) = 2.32$. The grey band encompasses 95 % of the sources and corresponds to a spread of $\Delta\Gamma_{\text{em}}^{\text{CP}} = 0.95$ above and below the horizontal fitting straight line. The total spread is 82 % of the value $\Gamma_{\text{em}}^{\text{CP}}(z) = 2.32$.

VI. AN ATTEMPT BASED ON AXION-LIKE PARTICLES

As an alternative possibility to implement our ideal scenario sketched in Section IV, we invoke new physics in the form of axion-like particles (ALPs). As discussed in the Appendix, their most characteristic feature is to couple only to two photons with a coupling constant $g_{a\gamma\gamma}$ according to the Feynman diagram shown in Fig. 6. Clearly, in the presence of the extragalactic magnetic field \mathbf{B} one photon line in Fig. 6 represents the \mathbf{B} field, and so we see that in such a situation energy-conserving oscillations between VHE gamma-rays and ALPs take place [21]. Accordingly, photons acquire a split personality, travelling for some time as real photons – which suffer EBL absorption – and for some time as ALPs, which are unaffected by the EBL (as explicitly shown in the Appendix). As a consequence, $\tau_{\gamma}(E_0, z)$ gets replaced by the effective optical depth $\tau_{\gamma}^{\text{eff}}(E_0, z)$, which is manifestly *smaller* than $\tau_{\gamma}(E_0, z)$ and is a monotonically increasing function of E_0 and z . The crux of the argument is that since the photon survival probability is now $P_{\gamma\rightarrow\gamma}^{\text{ALP}}(E_0, z) = e^{-\tau_{\gamma}^{\text{eff}}(E_0, z)}$, even a *small* decrease of $\tau_{\gamma}^{\text{eff}}(E_0, z)$ with respect to $\tau_{\gamma}^{\text{FRV}}(E_0, z)$ gives rise to a *large* increase of the photon survival probability, as compared to the case of conventional physics. So, the main consequence of photon-ALP oscillations is to *substantially attenuate* the EBL absorption.

Actually, $P_{\gamma\rightarrow\gamma}^{\text{ALP}}(E_0, z)$ can be computed exactly as outlined in the Appendix, where it is explained that the extragalactic magnetic field has a domain-like structure (at least in first approxi-

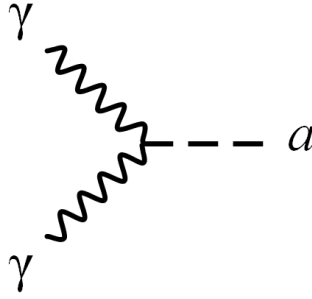


FIG. 6: Feynman diagram for the two-photon ALP coupling.

mation), namely that \mathbf{B} is homogeneous over a domain of size L_{dom} and has approximately the same strength B in all domains, but its direction randomly changes from one domain to another [29–31] (more about this, in the Appendix). Furthermore, it will be shown that the considered ALP scenario contains only two free parameters $\xi \propto g_{a\gamma\gamma} B$ and L_{dom} : they obviously show up in $P_{\gamma \rightarrow \gamma}^{\text{ALP}}(E_0, z)$ even though such a dependence is not exhibited for notational simplicity. Realistic values of these parameters are $\xi = 0.1, 0.5, 1, 5$ and $L_{\text{dom}} = 4 \text{ Mpc}, 10 \text{ Mpc}$, which will be regarded as our benchmark values. In reality, a third free parameter is the ALP mass m , but we assume $m < 10^{-9} \text{ eV}$ which entails that $P_{\gamma \rightarrow \gamma}^{\text{ALP}}(E_0, z)$ is *independent* of m (as discussed in the Appendix).

At this point, knowing $P_{\gamma \rightarrow \gamma}^{\text{ALP}}(E_0, z)$, we proceed as above. To wit, we first write the emitted flux of every source as

$$\Phi_{\text{em}}(E_0(1+z)) = \left(P_{\gamma \rightarrow \gamma}^{\text{ALP}}(E_0, z) \right)^{-1} K_{\text{obs}}(z) E_0^{-\Gamma_{\text{obs}}(z)}, \quad (5)$$

and next we best-fit this function to the single power-law $K_{\text{em}}^{\text{ALP}}(z) [(1+z)E_0]^{-\Gamma_{\text{em}}^{\text{ALP}}(z)}$ over the energy range ΔE_0 where the source is observed. This procedure is performed for each benchmark value of ξ and L_{dom} . We report in Table IV the values of $\Gamma_{\text{em}}^{\text{ALP}}$ for all the observed VHE blazars and for $L_{\text{dom}} = 4 \text{ Mpc}$, $\xi = 0.1, 0.5, 1, 5$, and similarly Table V contains the values of $\Gamma_{\text{em}}^{\text{ALP}}$ for all the observed VHE blazars and for $L_{\text{dom}} = 10 \text{ Mpc}$, $\xi = 0.1, 0.5, 1, 5$. Next, we carry out a statistical analysis of the values of $\Gamma_{\text{em}}^{\text{ALP}}(z)$ as a function of z , again for any benchmark value of ξ and L_{dom} . We still use the least square method and we try to fit the data with one parameter (horizontal line), two parameters (first-order polynomial) and three parameters (second-order polynomial). Finally, in order to quantify the statistical significance of each fit we compute the χ_{red}^2 , whose values are reported in Table I for $L_{\text{dom}} = 4 \text{ Mpc}$, $\xi = 0.1, 0.5, 1, 5$, and in Table II for $L_{\text{dom}} = 10 \text{ Mpc}$, $\xi = 0.1, 0.5, 1, 5$.

Hence, we see that the minimal χ_{red}^2 corresponds to the choices $\xi = 1$, $L_{\text{dom}} = 4 \text{ Mpc}$ and $\xi = 0.5$, $L_{\text{dom}} = 10 \text{ Mpc}$, which are therefore the values of ξ and L_{dom} – among our benchmark ones – which best-fit the data. Moreover, in either case data are best-fitted by an *horizontal* straight regression line, whose equation is $\Gamma_{\text{em}}^{\text{ALP}}(z) = 2.55$ for $\xi = 1$, $L_{\text{dom}} = 4 \text{ Mpc}$ and $\Gamma_{\text{em}}^{\text{ALP}}(z) = 2.52$ for $\xi = 0.5$, $L_{\text{dom}} = 10 \text{ Mpc}$.

Just like in Section III, we want to check the robustness of our conclusions by repeating the same statistical exercise *without* the BL Lac 1ES 0229+200. In this case, we find that for $L_{\text{dom}} = 4 \text{ Mpc}$ the best-fitting procedure singles out $\xi = 0.5$ and the best-fit *horizontal* straight regression line with equation $\Gamma_{\text{em}}^{\text{ALP}}(z) = 2.52$ with $\chi_{\text{red}}^2 = 1.43$, whereas for $L_{\text{dom}} = 10 \text{ Mpc}$ we get again $\xi = 0.5$ and the best-fit *horizontal* straight regression line with equation $\Gamma_{\text{em}}^{\text{ALP}}(z) = 2.58$ with $\chi_{\text{red}}^2 = 1.39$.

# of fit parameters	$\chi_{\text{red,CP}}^2$	$\chi_{\text{red,ALP}}^2$			
		$\xi = 0.1$	$\xi = 0.5$	$\xi = 1$	$\xi = 5$
1	4.03	3.93	2.33	2.16	2.54
2	3.49	3.45	2.39	2.21	2.58
3	3.56	3.50	2.34	2.26	2.64

TABLE I: The values of χ_{red}^2 are displayed for the three fitting models considered in the text. In the first column the number of parameters in each fitting model is reported. The second column concerns deabsorption according to conventional physics, using the EBL model of FRV. The other column pertains to the photon-ALP oscillation scenario with the EBL still described by the FRV model, and exhibits the values of χ_{red}^2 for $L_{\text{dom}} = 4$ Mpc and different choices of ξ . The value in bold-face is the minimum of χ_{red}^2 .

# of fit parameters	$\chi_{\text{red,CP}}^2$	$\chi_{\text{red,ALP}}^2$			
		$\xi = 0.1$	$\xi = 0.5$	$\xi = 1$	$\xi = 5$
1	4.03	3.69	2.10	2.34	2.56
2	3.49	3.35	2.15	2.39	2.60
3	3.56	3.36	2.19	2.44	2.66

TABLE II: Same as Table I, but with $L_{\text{dom}} = 10$ Mpc. The value in bold-face is the minimum of χ_{red}^2 .

As in the situation discussed in Section III, the quality of the fit is strongly improved, but the previous result is basically unchanged.

Quite remarkably, the logic underlying the present ALP picture naturally leads to the full implementation of our ideal scenario sketched in Section IV. Let us address this point in some detail.

- The existence of an ALP with suitable realistic values of the parameters which give rise to photon-ALP oscillations in extragalactic space yields a best-fit straight regression line for the values of $\Gamma_{\text{em}}^{\text{ALP}}(z)$ which is just *horizontal*, in perfect agreement with the first demand of our scenario. We stress that this is an *automatic* consequence of the present model, and not an *ad hoc* requirement as in the case discussed in Section IV. The situation is illustrated in Figs. 7. Moreover, the best-fitting demand also fixes $\xi \propto g_{a\gamma\gamma} B$ for any given value of L_{dom} .
- The tight correlation between $F_{\text{em},\Delta E}^{\text{CP}}(z)$ and $K_{\text{em}}^{\text{CP}}(z)$ found in the context of conventional physics persists in the presence of photon-ALP oscillations, as shown in Fig. 8. While it is fairly obvious that the upper and lower rows of Fig. 7 are almost indistinguishable, it comes instead as a real surprise that Figs. 4 and 8 look very similar. As a consequence, the scatter in the values of $\Gamma_{\text{em}}^{\text{ALP}}(z)$ must be small. Incidentally, it would be unphysical to require all our blazars to have precisely the same value of $\Gamma_{\text{em}}^{\text{ALP}}(z)$: any two identical galaxies have never been seen, but in addition some sources could be flaring while others could be quiescent. Thus, a small scatter in the values of $\Gamma_{\text{em}}^{\text{ALP}}(z)$ is physically compelling. Actually, in order to encompass 95% of the observed sources a spread of $\Delta\Gamma_{\text{em}}^{\text{ALP}} = 0.36$ both above and below the best-fit horizontal regression lines with either $\Gamma_{\text{em}}^{\text{ALP}}(z) = 2.52$ or $\Gamma_{\text{em}}^{\text{ALP}}(z) = 2.55$ is demanded. In both cases, the value of the total spread amounts to 28% of the best-fit value 2.52 or 2.55. This is represented by the grey band in right panels of Fig. 7. Hence, we see that – at variance with the attempt discussed in Section V – now the strip in question is thin enough to preserve the tight correlation between $F_{\text{em},\Delta E}^{\text{ALP}}(z)$ and $K_{\text{em}}^{\text{ALP}}(z)$.

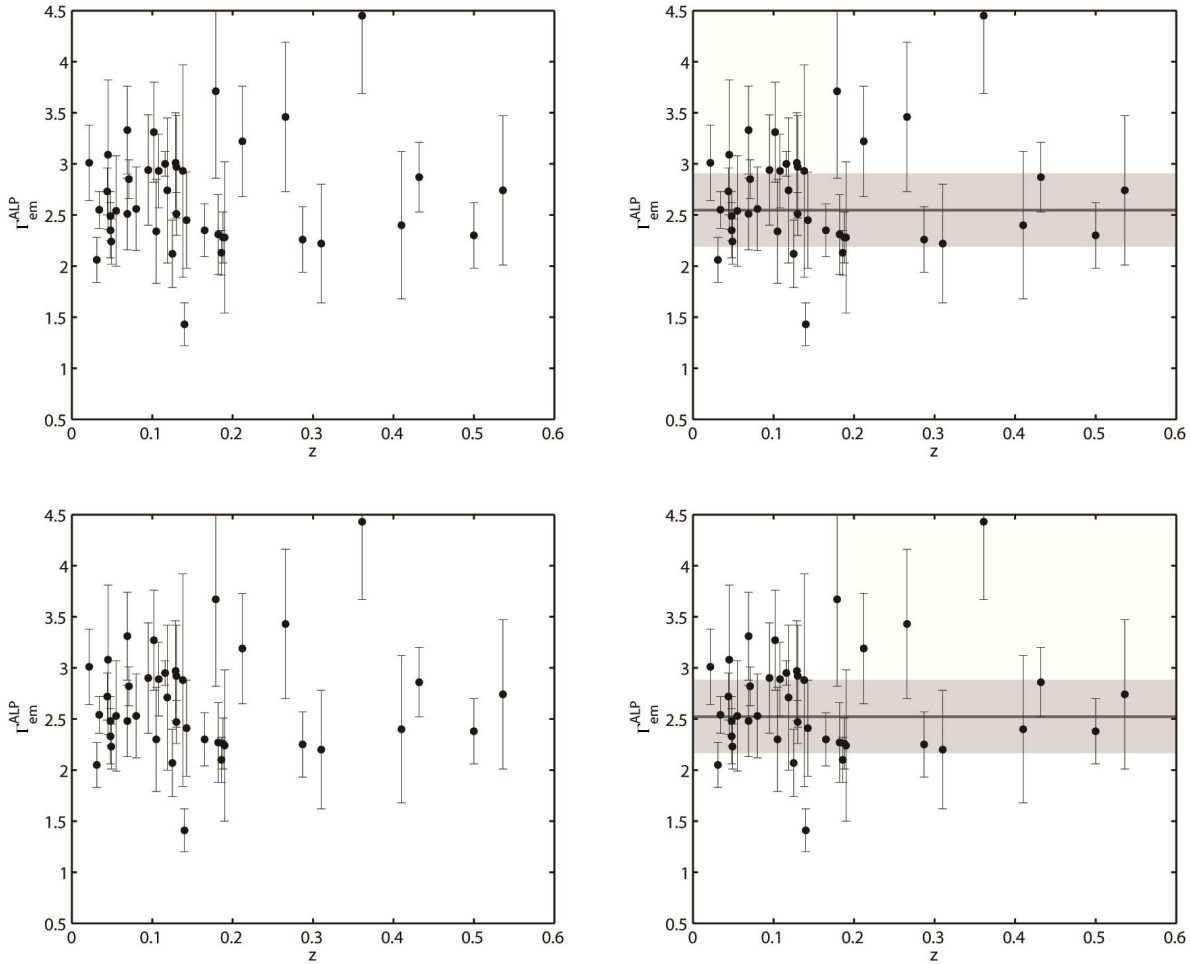


FIG. 7: Emitted spectral index $\Gamma_{\text{em}}^{\text{ALP}}(z)$ and best-fit straight regression line in the ALP scenario. The *upper row* corresponds to the case $\xi = 1$, $L_{\text{dom}} = 4$ Mpc while the *lower row* to $\xi = 0.5$, $L_{\text{dom}} = 10$ Mpc. *Left panels*: The values of $\Gamma_{\text{em}}^{\text{ALP}}(z)$ are plotted versus the source redshifts z for all our blazars with the corresponding error bars. *Right panels*: Same as left corresponding panels, but with superimposed the best-fit horizontal regression line. Moreover, the grey band encompasses 95% of the sources and corresponds to a spread of $\Delta\Gamma_{\text{em}}^{\text{ALP}} = 0.36$ above and below the best-fit regression line. The total spread is 28% of the value $\Gamma_{\text{em}}^{\text{ALP}}(z)$ in either case.

VII. DISCUSSION AND CONCLUSIONS

In this paper we have performed a comparative analysis of all blazars observed at the time of writing as far as a possible correlation between their VHE emitted spectra and their redshift is concerned.

Working within conventional physics, such a correlation has indeed emerged in the form of a peculiar z -dependence of the $\Gamma_{\text{em}}^{\text{CP}}(z)$ distribution, quantified by its best-fit straight regression line $\Gamma_{\text{em}}^{\text{CP}}(z) = 2.61 - 2.35z$ shown in the right panel of Fig. 3, which has $\chi_{\text{red}}^2 = 3.49$. However, this result brings out a serious drawback of the conventional scenario, which surprisingly has not previously been noticed. Indeed, such a correlation looks at odd with the lack of substantial cosmological evolutionary effects. Moreover, we have demonstrated that it is unphysical, because of two distinct

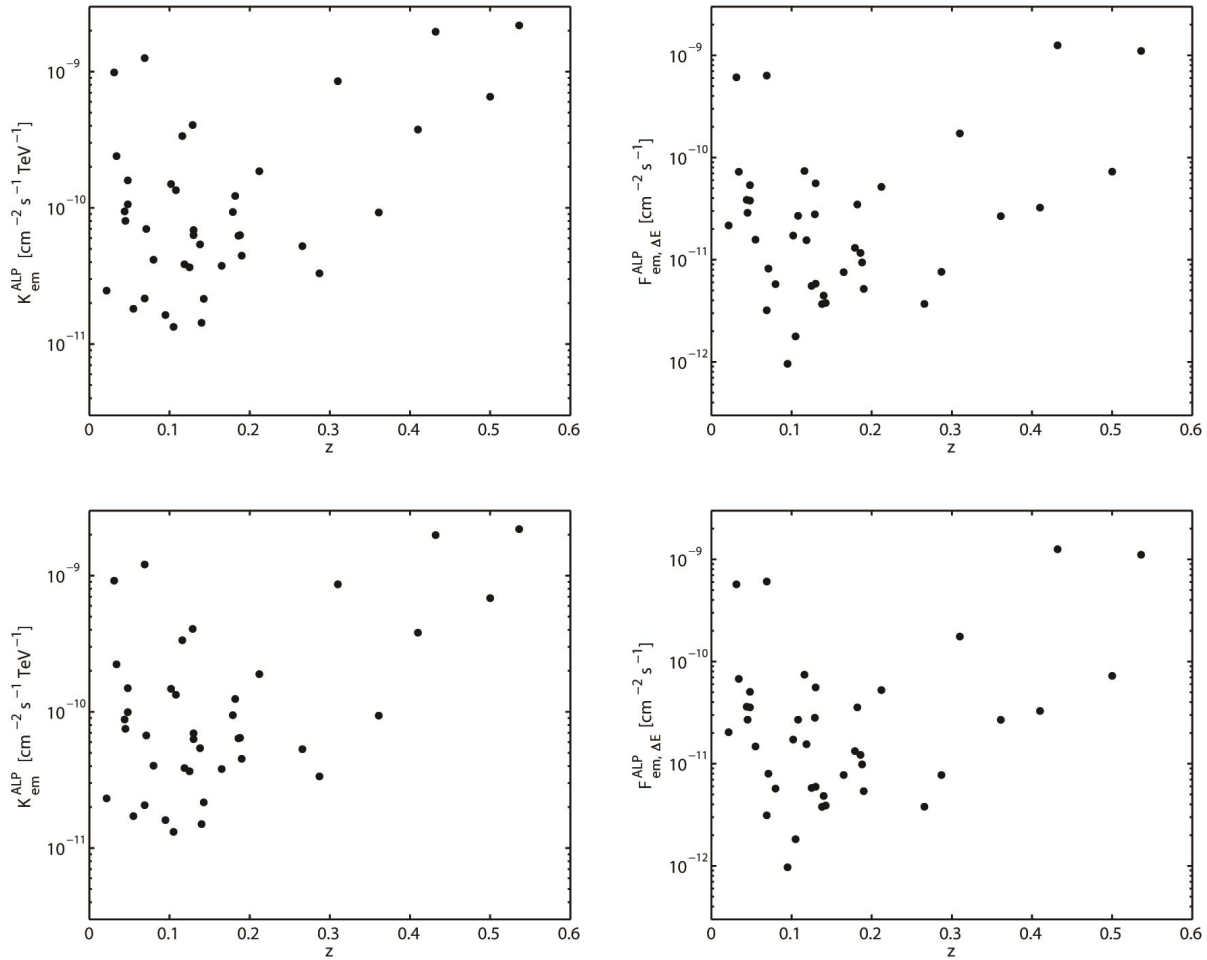


FIG. 8: Emitted flux normalization constant $K_{\text{em}}^{\text{ALP}}(z)$ and emitted flux $F_{\text{em},\Delta E}^{\text{ALP}}(z)$ inside ΔE in the ALP scenario. The *upper row* corresponds to the case $\xi = 1$, $L_{\text{dom}} = 4 \text{ Mpc}$ while the *lower row* to $\xi = 0.5$, $L_{\text{dom}} = 10 \text{ Mpc}$. *Left panels*: The values of $K_{\text{em}}^{\text{ALP}}(z)$ are plotted versus the source redshift z for all our blazars. *Right panels*: The values of $F_{\text{em},\Delta E}^{\text{ALP}}(z)$ are plotted versus the source redshift z for all blazars considered in the corresponding left panels.

reasons.

- It implies that blazars with harder emitted spectra are observed *only* at larger redshifts.
- It upsets the tight correlation found between $F_{\text{em},\Delta E}^{\text{CP}}(z)$ and $K_{\text{em}}^{\text{CP}}(z)$.

Next, we have identified the characteristic features that an ideal scenario should possess in order to be physically consistent as far as the correlation in question is concerned. Basically, the distribution of $\Gamma_{\text{em}}(z)$ as a function of z should have an almost horizontal best-fit straight regression line and the values of $\Gamma_{\text{em}}(z)$ for all sources should have a small scatter about it.

We have also explicitly shown that such a scenario cannot be implemented within conventional physics, where the large scatter in the values of both $K_{\text{em}}^{\text{CP}}(z)$ and $\Gamma_{\text{em}}^{\text{CP}}(z)$ is an intrinsic property of blazars, which vary from source to source. We are thus inescapably led to the conclusion that the conventional scenario is affected by a serious physical shortcoming.

In an effort to implement our ideal scenario, we have considered a framework where new physics in the form of ALPs is present, with photon-ALP oscillations taking place in the extragalactic magnetic field. Their result is ultimately to substantially reduce the level of EBL absorption. We have focussed our attention on two realistic benchmark cases: $L_{\text{dom}} = 4 \text{ Mpc}$ and $L_{\text{dom}} = 10 \text{ Mpc}$. After having worked out the effect of photon-ALP oscillations on the VHE emitted spectra starting from the observed ones, we have discovered that in either case the best-fit regression line of the values of $\Gamma_{\text{em}}^{\text{ALP}}(z)$ for all considered blazars turns out to be a straight line *independent* of z , as shown in the right panels of Fig. 7. This looks astonishing. Of course, by changing the effective level of EBL absorption we obviously expect the z -dependence of the $\Gamma_{\text{em}}^{\text{ALP}}(z)$ distribution to differ from that of the $\Gamma_{\text{em}}^{\text{CP}}(z)$ distribution. In other words, the inclination of the best-fit straight regression line in the $\Gamma_{\text{em}} - z$ plane should change. But to become horizontal – which is barely the only possibility in agreement with physical expectation – looks almost like a miracle. In addition, the values of $\Gamma_{\text{em}}^{\text{ALP}}(z)$ for the individual sources turn out to have a small scatter about the considered best-fit straight regression line, and so the tight correlation between $F_{\text{em},\Delta E}^{\text{ALP}}(z)$ and $K_{\text{em}}^{\text{ALP}}(z)$ – found also in the present context – is preserved (see Fig. 8). Thus, we see that our ideal scenario is here successfully implemented.

Actually, the considered ALP framework possesses further nice features. Even from a purely statistical point of view it is better than the conventional scenario, in which we have found $\chi_{\text{red}}^2 = 3.49$ for the best-fit straight regression line (Section III) or $\chi_{\text{red}}^2 = 4.03$ for the horizontal fitting straight line (Section V). Instead now the best-fit straight regression lines in the right panels of Fig. 7 have $\chi_{\text{red}}^2 = 2.16$ for $L_{\text{dom}} = 4 \text{ Mpc}$ and $\chi_{\text{red}}^2 = 2.10$ for $L_{\text{dom}} = 10 \text{ Mpc}$. From a physical standpoint instead, a new picture arises wherein a sharp distinction between fundamental physics and boundary conditions can naturally emerge. Indeed, the small scatter in the values of $\Gamma_{\text{em}}^{\text{ALP}}(z)$ implies that the emission mechanism is basically identical for all sources. On the other hand, the large scatter in the values of $K_{\text{em}}^{\text{ALP}}(z)$ – nearly unaffected by photon-ALP oscillations – is naturally traced back to the largely different environmental state of each source, such as for instance the accretion rate. A natural question should finally be addressed. How is it possible that the large scatter in $\Gamma_{\text{obs}}(z)$ exhibited in Fig. 1 arises from the small scatter in $\Gamma_{\text{em}}^{\text{ALP}}(z)$ as shown in the right panels of Fig. 7? The answer is very simple: most of the scatter in $\Gamma_{\text{obs}}(z)$ arises from the large scatter in the source distance.

Before closing this Section, we find it worthwhile to put the result of our investigation into its proper perspective.

During the last decade the interest in ALPs has been steadily growing. Various reasons have conspired towards this circumstance. With different motivations, the astrophysical implications of ALPs have been addressed since twenty years [32–39]. Certainly the claimed discovery of an ALP by the PVLAS collaboration [40] in 2005, which – even if subsequently withdrawn by the PVLAS collaboration itself [41] – has provided a stimulus to look for astrophysical cross-checks [42–46]. Soon thereafter, it has been realized that several superstring theories predict the existence of not only a single kind of ALP but more generally of a family of ALPs with very small masses [10–19]. As a matter of fact, the study of the relevance of ALPs for high-energy astrophysics has continued until the present [21, 47–84].

A tension between the predicted EBL level causing photon absorption and observations in the VHE range has been claimed from time to time (see e.g. [85, 86]), but then a better determination of the EBL properties has shown that no problem exists. As already stressed at the beginning of Section III, nowadays the situation is different, since different techniques basically lead to the same EBL model. Yet, it has recently been claimed that VHE observations require an EBL level even lower than that predicted by the minimal EBL model normalized to the galaxy counts only [87]. This is the so-called *pair-production anomaly*, which is based on the Kolmogorov test and so does not rely upon the estimated errors. It has thoroughly been quantified by a global statistical analysis

of a large sample of observed blazars, showing that measurements in the regime of large optical depth deviate by 4.2σ from measurements in the optically thin regime [63]. Systematic effects have been shown to be insufficient to account for such the pair-production anomaly, which looks therefore real. Actually, the discovery of new blazars at large redshift like the observation of PKS 1424+240 have strengthened the case for the pair-production anomaly [75]. Quite recently, the existence of the pair-production anomaly has been questioned by using a new EBL model and a ξ^2 test, in which errors play instead an important role [88]. Because the Kolmogorov test looks more robust in that it avoids taking errors into account, we tend to believe that the pair-production anomaly is indeed at the level of 4.2σ .

Amazingly, the existence of photon-ALP oscillations with the *same* realistic choice of the model parameters provides an excellent explanation for three *completely different* phenomena occurring in the VHE band.

- The pair-production anomaly is naturally explained in terms of photon-ALP oscillations in extragalactic magnetic fields [63, 71, 75]. This should hardly come as surprise, since – as already explained – the ultimate effect of photon-ALP oscillation is to substantially lower the effective EBL absorption level.
- According to conventional physics, flat spectrum radio quasars (FSRQs) should not emit above 20 – 30 GeV. This is due to the fact that higher energy photons accelerated in the jet enter – at a distance of about 1 kpc from the centre – the so-called broad-line region (BLR), whose high density of ultraviolet photons gives rise to an optical depth $\tau \simeq 15$ owing to the same $\gamma\gamma \rightarrow e^+e^-$ absorption process considered above. Even in this context, photon-ALP oscillations substantially lower the photon absorption level inside the BLR while still staying inside the standard blazar models, thereby allowing VHE photons to escape the BLR and be emitted, in remarkable quantitative agreement with observations [67]. We stress that the detection of VHE photons from FSRQs still represents a serious challenge for conventional models.
- Our findings described in the present paper show that the conventional scenario of photon propagation in extragalactic space is seriously challenged. Nevertheless, a physically satisfactory picture emerges by considering photon-ALP oscillations in the extragalactic magnetic field.

Altogether, such a situation evidently strongly suggests a preliminary evidence for the existence of an ALP, whose parameters make it a good candidate for cold dark matter [20]. Moreover, it looks tantalizing that the issue can definitively be settled both with the advent of the new gamma-ray detectors like the CTA [89] as well as with the planned laboratory experiment ALPS II at DESY [90, 91] and IAXO (International Axion Telescope) [91, 92] which will have the capability to discover an ALP with the properties assumed in the present analysis. Also experiments exploiting the techniques discussed in [93–95] are quite promising for the laboratory detection of an ALP of this kind.

ACKNOWLEDGMENTS

We thank Patrizia Caraveo for useful discussions. We also thank Abelardo Moralejo, Georg Raffelt, Andreas Ringwald and Fabrizio Tavecchio for their comments. The work of M. R. is supported by INFN TAsP and CTA grants.

APPENDIX

Here we summarize the main properties of the ALP scenario considered in the text and the evaluation of the photon survival probability $P_{\gamma \rightarrow \gamma}^{\text{ALP}}(E_0, z)$.

A. General properties of axion-like particles (ALPs)

As already stated, ALPs are spin-zero, neutral and extremely light pseudo-scalar bosons similar to the *axion*, namely the pseudo-Goldstone boson associated with the global Peccei-Quinn symmetry $U(1)_{\text{PQ}}$ proposed as a natural solution to the strong CP problem [96]. The axion interacts with fermions, two gluons and two photons, and one of its characteristic feature is the existence of a strict linear relationship between its mass m and the two-photon coupling constant $g_{a\gamma\gamma}$

$$m = 0.7 k \left(g_{a\gamma\gamma} 10^{10} \text{ GeV} \right) \text{ eV} , \quad (6)$$

where k is a model-dependent constant of order 1 [97]. Nevertheless, ALPs differ from axions in two respects: (1) their mass m and two-photon coupling constant $g_{a\gamma\gamma}$ are *unrelated*, and (2) ALPs are supposed to interact *only* with two photons [9]. Hence, they are described by the Lagrangian

$$\mathcal{L}_{\text{ALP}} = \frac{1}{2} \partial^\mu a \partial_\mu a - \frac{1}{2} m^2 a^2 - \frac{1}{4} g_{a\gamma\gamma} F_{\mu\nu} \tilde{F}^{\mu\nu} a = \frac{1}{2} \partial^\mu a \partial_\mu a - \frac{1}{2} m^2 a^2 + g_{a\gamma\gamma} \mathbf{E} \cdot \mathbf{B} a , \quad (7)$$

where a and m are the ALP field and mass, respectively, and \mathbf{E} and \mathbf{B} are the electric and magnetic components of the field strength $F_{\mu\nu}$ ($\tilde{F}^{\mu\nu}$ is its dual).

We shall be concerned with the particular case of a monochromatic photon/ALP beam emitted by a blazar at redshift z and traveling through the ionized extragalactic space, where a magnetic field \mathbf{B} is supposed to exist with the domain-like structure described in Section VI. Therefore \mathbf{E} is the electric field of a beam photon while \mathbf{B} is the extragalactic magnetic field. In such a situation, the mass matrix of the photon-ALP system is non-diagonal, so that the propagation eigenstates differ from the interaction eigenstates. This fact gives rise to photon-ALP oscillations in the beam [98, 99], much in the same way as it happens in a beam of massive neutrinos of different flavor (however for photon-ALP oscillations an external magnetic field is needed to compensate for the spin mismatch). In order to avoid notational confusion, the symbol E will henceforth denote the energy of the beam particles.

Since we suppose that $E \gg m$ (more about this, later), we can employ the *short wavelength approximation*. As a consequence, the photon/ALP beam propagation turns out to be described by the following first-order Schrödinger-like equation with the time replaced by the y -coordinate along the beam [99]

$$\left(i \frac{d}{dy} + E + \mathcal{M} \right) \psi(y) = 0 \quad (8)$$

with wave function

$$\psi(y) \equiv \begin{pmatrix} A_x(y) \\ A_z(y) \\ a(y) \end{pmatrix} , \quad (9)$$

where $A_x(y)$ and $A_z(y)$ denote the photon amplitudes with polarization along the x - and z -axis, respectively, while $a(y)$ is the amplitude associated with the ALP. It is useful to introduce the 3-dimensional basis vectors $\{|\gamma_x\rangle, |\gamma_z\rangle, |a\rangle\}$ where $|\gamma_x\rangle \equiv (1, 0, 0)^T$ and $|\gamma_z\rangle \equiv (0, 1, 0)^T$ represent

the two photon linear polarization states along the x - and z -axis, respectively, and $|a\rangle \equiv (0, 0, 1)^T$ denotes the ALP state. Accordingly, we can write $\psi(y)$ as

$$\psi(y) = A_x(y) |\gamma_x\rangle + A_z(y) |\gamma_z\rangle + a(y) |a\rangle . \quad (10)$$

Note that the quantity $\mathcal{H} \equiv -(E + \mathcal{M})$ plays formally the role of the Hamiltonian. Denoting by $\mathcal{U}(y, y_0)$ the transfer matrix – namely the solution of Eq. (8) with initial condition $\mathcal{U}(y_0, y_0) = 1$ – the propagation of a generic wave function across the domain in question can be represented as

$$\psi(y) = \mathcal{U}(y, y_0) \psi(y_0) . \quad (11)$$

So far our attention has been restricted to the wave function, which describes a polarized beam. However, since in the gamma-ray band the polarization cannot be measured, we are forced to employ the density matrix $\rho(y)$. As in quantum mechanics, it obeys the analog of the Von Neumann equation associated with Eq. (8), whose form is

$$i \frac{d\rho}{dy} = \rho \mathcal{M}^\dagger - \mathcal{M} \rho . \quad (12)$$

As we shall see, EBL absorption implies that \mathcal{H} – and so \mathcal{M} and $\rho(y)$ – are not self-adjoint. Hence $\mathcal{U}(y, y_0)$ fails to be unitary. Nevertheless, it is trivial to check that the familiar relation

$$\rho(y) = \mathcal{U}(y, y_0) \rho(y_0) \mathcal{U}^\dagger(y, y_0) \quad (13)$$

retains its validity. Moreover, the probability that the beam in the state ρ_1 at y_0 will be found in the state ρ_2 at y is still given by the standard relation

$$P_{\rho_1 \rightarrow \rho_2}(y_0, y) = \text{Tr}(\rho_2 \mathcal{U}(y, y_0) \rho_1(y_0) \mathcal{U}^\dagger(y, y_0)) , \quad (14)$$

where it is supposed as usual that $\text{Tr} \rho_1 = \text{Tr} \rho_2 = 1$.

We stress that the advantage arising from the short wavelength approximation is that the beam propagation can *formally* be described as a three-level non-relativistic decaying quantum system.

It is quite enlightening to start by considering the beam propagation over a single magnetic domain and to neglect EBL absorption [49, 99] (this attitude indeed makes sense, since EBL absorption is independent of photon-ALP oscillations). Because then \mathbf{B} is homogeneous, we can choose the z -axis along \mathbf{B} so that $B_x = 0$. Correspondingly, the matrix \mathcal{M} entering Eq. (8) takes the form

$$\mathcal{M} = \begin{pmatrix} -\omega_{\text{pl}}^2/2E & 0 & 0 \\ 0 & -\omega_{\text{pl}}^2/2E & g_{a\gamma\gamma} B/2 \\ 0 & g_{a\gamma\gamma} B/2 & -m^2/2E \end{pmatrix} , \quad (15)$$

where ω_{pl} is the plasma frequency of the ionized intergalactic medium (IGM), which is related to the mean electron density n_e by $\omega_{\text{pl}} = 3.69 \cdot 10^{-11} (n_e/\text{cm}^{-3})^{1/2} \text{ eV}$ [99]. So, by defining the oscillation wave number as

$$\Delta_{\text{osc}} \equiv \left[\left(\frac{m^2 - \omega_{\text{pl}}^2}{2E} \right)^2 + (g_{a\gamma\gamma} B)^2 \right]^{1/2} , \quad (16)$$

it is a simple exercise to show that the photon-ALP conversion probability across the considered domain is

$$P_{\gamma \rightarrow a}(L_{\text{dom}}) = \left(\frac{g_{a\gamma\gamma} B}{\Delta_{\text{osc}}} \right)^2 \sin^2 \left(\frac{\Delta_{\text{osc}} L_{\text{dom}}}{2} \right) . \quad (17)$$

Thus, defining the energy threshold [49]

$$E_L \equiv \frac{|m^2 - \omega_{\text{pl}}^2|}{2 g_{a\gamma\gamma} B} , \quad (18)$$

we see that in the *strong-mixing regime* – namely when condition $E > E_L$ is met – Eq. (16) reduces to

$$\Delta_{\text{osc}} \simeq g_{a\gamma\gamma} B \quad (19)$$

and consequently the photon-ALP conversion probability becomes maximal as well as *energy-independent*. Finally, since $g_{a\gamma\gamma}$ and B enter \mathcal{L}_{ALP} only in the combination $g_{a\gamma\gamma} B$, it proves instrumental to define the quantity

$$\xi \equiv \left(\frac{B}{\text{nG}} \right) (g_{a\gamma\gamma} 10^{11} \text{ GeV}) , \quad (20)$$

in terms of which Eq. (18) can be rewritten as

$$E_L \simeq \frac{25.64}{\xi} \left| \left(\frac{m}{10^{-10} \text{ eV}} \right)^2 - \left(\frac{\omega_{\text{pl}}}{10^{-10} \text{ eV}} \right)^2 \right| \text{ GeV} . \quad (21)$$

B. Model parameters

Before proceeding further, it is worthwhile to discuss the allowed values of the free parameters of the model. In this field, a signal is considered a discovery if its statistical significance is at least 5σ . Accordingly, the bounds should be divided into two classes, depending on whether their statistical significance is larger or smaller than 5σ .

- Those with statistical significance *larger* than 5σ prevent any discovery of an ALP, and to date only one bound belongs to this class: the one obtained by the CAST experiment at CERN, which reads $g_{a\gamma\gamma} < 8.8 \cdot 10^{-11} \text{ GeV}$ for $m < 0.02 \text{ eV}$ [100].
- All other weaker bounds provide useful information, but still allow for the discovery of an ALP. Various bounds of this sort have been derived, but we discuss here only those that we believe to be most relevant. One is based on the study of 39 Galactic globular clusters and slightly improves the CAST constraint giving $g_{a\gamma\gamma} < 6.6 \cdot 10^{-11} \text{ GeV}$ at the 2σ level (the mass range of its validity is not specified) [78]. Another has been obtained by the H.E.S.S. collaboration, looking at the source PKS 2155 – 304, from the absence of the characteristic fluctuating behavior of the realizations of the beam propagation around E_L (more about this, later) and reads $g_{a\gamma\gamma} < 2.1 \cdot 10^{-11} \text{ GeV}$ for $1.5 \cdot 10^{-8} \text{ eV} < m < 6.0 \cdot 10^{-8} \text{ eV}$ at the 2σ level [72]. A similar strategy has been applied to the source to the Hydra galaxy cluster, yielding $g_{a\gamma\gamma} < 8.3 \cdot 10^{-12} \text{ GeV}$ for $\text{eV} < m < 7.0 \cdot 10^{-12} \text{ eV}$ at the 2σ level [73]. Finally, the explosion of the 1987A supernova has been used to set an upper bound on $g_{a\gamma\gamma}$ depending on the value of m . The logic is as follows. Along with a neutrino burst lasting about 10 seconds, also an ALP burst should be emitted during the collapse. Inside the Galaxy magnetic field, some of the ALPs should convert into X-rays and next be detected by the Solar Maximal Mission (SMM) satellite. From the absence of detection, originally the bounds $g_{a\gamma\gamma} < 1.0 \cdot 10^{-11} \text{ GeV}$ for $m < 1.0 \cdot 10^{-9} \text{ eV}$ [33] and $g_{a\gamma\gamma} < 3.0 \cdot 10^{-12} \text{ GeV}$ for $m < 1.0 \cdot 10^{-9} \text{ eV}$ have been set [34]. A very recent analysis updating these two early works has been carried out, especially using the present state-of-the art knowledge of supernova

explosions (even if we still do not know why they actually explode). However, an unavoidable uncertainty affects the detection efficiency of the SMM, for instance the systematic error and the effective area, even because SN1987A was observed perpendicularly to the viewing direction of the SMM. The authors do not quote the statistical significance of this bound, which is certainly less than 2σ [84].

As far as the extragalactic magnetic field \mathbf{B} is concerned, the situation is much less clear-cut. A general consensus exists that it possesses a domain-like morphology (at least in first approximation) [29–31]. As mentioned in Section IV, it is supposed that \mathbf{B} is homogeneous over a domain of size L_{dom} equal to its coherence length, with \mathbf{B} *randomly* changing its direction from one domain to another but keeping approximately the same strength. Unfortunately, the values of both B and L_{dom} are largely unknown. We assume B to be pretty large according to the predictions of the galactic outflows models [101, 102]. Actually, within these models it looks natural to suppose that L_{dom} is of the order of the galactic correlation length, which amounts to take $L_{\text{dom}} = (1 - 10)$ Mpc in the present Universe ($z = 0$), even though larger values cannot be excluded. Then Fig. 4 of [103] implies that $B \leq 1$ nG, and so by taking the most restrictive bound on $g_{a\gamma\gamma}$ it follows from Eq. (20) that $\xi < 8$. The upper bound on the mean diffuse extragalactic electron density $n_e < 2.7 \cdot 10^{-7} \text{ cm}^{-3}$ is provided by the WMAP measurement of the baryon density [104], which – thanks to the above relation – translates into the upper bound $\omega_{\text{pl}} < 1.92 \cdot 10^{-14} \text{ eV}$. What about m ? In order to maximize the effect of photon-ALP oscillations we work throughout within the strong mixing regime. Recalling that the lower end of the VHE band is $E = 100 \text{ GeV}$, we then have to require $E_L < 100 \text{ GeV}$. Putting everything together and using Eq. (21) we find $m < 1.97 \cdot 10^{-10} \xi^{1/2}$, and at any rate we should have $m < 5 \cdot 10^{-10} \text{ eV}$. However, we remark that the size of the effect remains basically unchanged if the bound $E_L < 100 \text{ GeV}$ becomes less restrictive by a factor of a few, and so for all practical purposes we can assume $m < 10^{-9} \text{ eV}$. Finally, by combining the CAST bound $g_{a\gamma\gamma} < 8.8 \cdot 10^{-11} \text{ GeV}$ with the interaction term in \mathcal{L}_{ALP} , it is straightforward to get the following order-of-magnitude estimate for the cross-sections $\sigma(a\gamma \rightarrow f^+f^-) \sim \sigma(a f^\pm \rightarrow \gamma f^\pm) < 10^{-50} \text{ cm}^2$ (here f denotes any charged fermion), which show that effectively ALPs do not interact with anything and in particular with the EBL.

C. Strategy

One point should now be emphasized. Due to the nature of the extragalactic magnetic field, the angle of \mathbf{B} in each domain with a fixed fiducial direction equal for all domains (which we identify with the z -axis) is a random variable, and so the propagation of the photon/ALP beam becomes a N_d -dimensional *stochastic process*, where N_d denotes the total number of magnetic domains crossed by the beam. Therefore we identify the photon survival probability with its average value. Moreover, we shall see that the whole photon/ALP beam propagation can be recovered by iterating N_d times the propagation over a single magnetic domain, changing each time the value of the random angle. Thanks to the fact that \mathbf{B} is homogeneous in every domain, the beam propagation equation can be solved exactly in a single domain. Clearly, at the end we have to average the photon survival probability as evaluated for one arbitrary realization of the whole propagation process – namely for a particular choice of the random angle in each domain – over all possible realizations of the considered stochastic process (i.e. over all values of the random angle in each of the N_d domains) [105].

Our discussion is framed within the standard Λ CDM cosmological model with $\Omega_M = 0.3$ and $\Omega_\Lambda = 0.7$, and so the redshift is the natural parameter to express distances. In particular, the

proper length $L_{\text{dom}}(z_a, z_b)$ extending over the redshift interval $[z_a, z_b]$ is

$$L(z_a, z_b) \simeq 4.29 \cdot 10^3 \int_{z_a}^{z_b} \frac{dz}{(1+z)[0.7+0.3(1+z)^3]^{1/2}} \text{Mpc} \simeq 2.96 \cdot 10^3 \ln \left(\frac{1+1.45 z_b}{1+1.45 z_a} \right) \text{Mpc}. \quad (22)$$

Accordingly, the overall structure of the cellular configuration of the extragalactic magnetic field is naturally described by a *uniform* mesh in redshift space with elementary step Δz , which is therefore the same for all domains. This mesh can be constructed as follows. We denote by $L_{\text{dom}}^{(n)} = L((n-1)\Delta z, n\Delta z)$ the proper length along the y -direction of the generic n -th domain, with $1 \leq n \leq N_d$, where the total number of magnetic domains N_d towards the considered blazar is the maximal integer contained in the number $z/\Delta z$, hence $N_d \simeq z/\Delta z$. In order to fix Δz we consider the domain closest to us, labelled by 1 and – with the help of Eq. (22) – we write its proper length as $(L_{\text{dom}}^{(1)}/5 \text{Mpc}) 5 \text{Mpc} = L(0, \Delta z) = 2.96 \cdot 10^3 \ln(1+1.45 \Delta z) \text{Mpc}$, from which we get $\Delta z \simeq 1.17 \cdot 10^{-3} (L_{\text{dom}}^{(1)}/5 \text{Mpc})$. So, once $L_{\text{dom}}^{(1)}$ is chosen in agreement with the previous considerations, the size of *all* magnetic domains in redshift space is fixed. At this point, two further quantities can be determined. First, the total number of the considered domains is $N_d \simeq z/\Delta z \simeq 0.85 \cdot 10^3 (5 \text{Mpc}/L_{\text{dom}}^{(1)}) z$. Second, the proper length of the n -th domain along the y -direction follows from Eq. (22) with $z_a \rightarrow (n-1)\Delta z, z_b \rightarrow n\Delta z$. Whence

$$L_{\text{dom}}^{(n)} \simeq 2.96 \cdot 10^3 \ln \left(1 + \frac{1.45 \Delta z}{1+1.45(n-1)\Delta z} \right) \text{Mpc}. \quad (23)$$

D. Propagation over a single domain

What still has to be done is to take EBL absorption into account and to determine the magnetic field strength $B^{(n)}$ in the generic n -th domain.

The first goal can be achieved by simply following the discussion of [105]. Because the domain size is so small as compared to the cosmological standards, we can safely drop cosmological evolutionary effects when considering a single domain. Then as far as absorption is concerned what matters is the mean free path λ_γ for the reaction $\gamma\gamma \rightarrow e^+e^-$, and the term $i/2\lambda_\gamma$ should be inserted into the 11 and 22 entries of the \mathcal{M} matrix. In order to evaluate λ_γ , we imagine that two hypothetical sources located at both edges of the n -th domain are observed. Therefore, we insert Eq. (2) into Eq. (1) of Section I and further apply the resulting equation to both of them. With the notational simplifications $\Phi_{\text{obs}}(E_0, z) \rightarrow \Phi(E_0)$ and $\Phi_{\text{em}}(E_0(1+z)) \rightarrow \Phi(E_0(1+z))$, we have

$$\Phi(E_0) = e^{-\tau_\gamma(E_0, (n-1)\Delta z)} \Phi(E_0[1+(n-1)\Delta z]), \quad \Phi(E_0) = e^{-\tau_\gamma(E_0, n\Delta z)} \Phi(E_0(1+n\Delta z)), \quad (24)$$

which upon combination imply that the flux change across the domain in question is

$$\Phi(E_0[1+(n-1)\Delta z]) = e^{-[\tau_\gamma(E_0, n\Delta z) - \tau_\gamma(E_0, (n-1)\Delta z)]} \Phi(E_0(1+n\Delta z)). \quad (25)$$

Because cosmological effects can be neglected across a single domain, Eq. (25) should have the usual form

$$\Phi(E_0[1+(n-1)\Delta z]) = e^{-L_{\text{dom}}^{(n)}/\lambda_\gamma^{(n)}(E_0)} \Phi(E_0, (1+n\Delta z)), \quad (26)$$

and the comparison with Eq. (25) ultimately yields

$$\lambda_\gamma^{(n)}(E_0) = \frac{L_{\text{dom}}^{(n)}}{\tau_\gamma(E_0, n\Delta z) - \tau_\gamma(E_0, (n-1)\Delta z)}, \quad (27)$$

where the optical depth is evaluated as stated in the text for the EBL model of FRV [22].

To accomplish the second task, we note that because of the high conductivity of the IGM medium the magnetic flux lines can be thought as frozen inside it [31]. Therefore the flux conservation during the cosmic expansion entails that B scales like $(1+z)^2$, so that the magnetic field strength in a domain at redshift z is $B(z) = B(z=0)(1+z)^2$. Hence in the n -th magnetic domain we have $B^{(n)} = B^{(1)}(1+(n-1)\Delta z)^2$.

So, at this stage the matrix \mathcal{M} in Eq. (8) as explicitly written in the n -th domain reads

$$\mathcal{M}^{(n)} = \begin{pmatrix} i/2\lambda_\gamma^{(n)} & 0 & B^{(n)} \sin \psi_n g_{a\gamma\gamma}/2 \\ 0 & i/2\lambda_\gamma^{(n)} & B^{(n)} \cos \psi_n g_{a\gamma\gamma}/2 \\ B^{(n)} \sin \psi_n g_{a\gamma\gamma}/2 & B^{(n)} \cos \psi_n g_{a\gamma\gamma}/2 & 0 \end{pmatrix}, \quad (28)$$

where ψ_n is the random angle between $\mathbf{B}^{(n)}$ and the fixed fiducial direction along the z -axis (note that indeed $\mathcal{M}^\dagger \neq \mathcal{M}$). Apart from ψ_n , all other matrix elements entering $\mathcal{M}^{(n)}$ are known. Finding the transfer matrix of Eq. (8) with $\mathcal{M}^{(n)}$ given by Eq. (28) is a straightforward even if somewhat boring game. The result is

$$\mathcal{U}_n(E_n, \psi_n) = e^{iE_n L_{\text{dom}}^{(n)}} \left[e^{i(\lambda_1^{(n)} L_{\text{dom}}^{(n)})} T_1(\psi_n) + e^{i(\lambda_2^{(n)} L_{\text{dom}}^{(n)})} T_2(\psi_n) + e^{i(\lambda_3^{(n)} L_{\text{dom}}^{(n)})} T_3(\psi_n) \right] \quad (29)$$

with

$$T_1(\psi_n) \equiv \begin{pmatrix} \cos^2 \psi_n & -\sin \psi_n \cos \psi_n & 0 \\ -\sin \psi_n \cos \psi_n & \sin^2 \psi_n & 0 \\ 0 & 0 & 0 \end{pmatrix}, \quad (30)$$

$$T_2(\psi_n) \equiv \begin{pmatrix} \frac{-1+\sqrt{1-4\delta_n^2}}{2\sqrt{1-4\delta_n^2}} \sin^2 \psi_n & \frac{-1+\sqrt{1-4\delta_n^2}}{2\sqrt{1-4\delta_n^2}} \sin \psi_n \cos \psi_n & \frac{i\delta_n}{\sqrt{1-4\delta_n^2}} \sin \psi_n \\ \frac{-1+\sqrt{1-4\delta_n^2}}{2\sqrt{1-4\delta_n^2}} \sin \psi_n \cos \psi_n & \frac{-1+\sqrt{1-4\delta_n^2}}{2\sqrt{1-4\delta_n^2}} \cos^2 \psi_n & \frac{i\delta_n}{\sqrt{1-4\delta_n^2}} \cos \psi_n \\ \frac{i\delta_n}{\sqrt{1-4\delta_n^2}} \sin \psi_n & \frac{i\delta_n}{\sqrt{1-4\delta_n^2}} \cos \psi_n & \frac{1+\sqrt{1-4\delta_n^2}}{2\sqrt{1-4\delta_n^2}} \end{pmatrix}, \quad (31)$$

$$T_3(\psi_n) \equiv \begin{pmatrix} \frac{1+\sqrt{1-4\delta_n^2}}{2\sqrt{1-4\delta_n^2}} \sin^2 \psi_n & \frac{1+\sqrt{1-4\delta_n^2}}{2\sqrt{1-4\delta_n^2}} \sin \psi_n \cos \psi_n & \frac{-i\delta_n}{\sqrt{1-4\delta_n^2}} \sin \psi_n \\ \frac{1+\sqrt{1-4\delta_n^2}}{2\sqrt{1-4\delta_n^2}} \sin \psi_n \cos \psi_n & \frac{1+\sqrt{1-4\delta_n^2}}{2\sqrt{1-4\delta_n^2}} \cos^2 \psi_n & \frac{-i\delta_n}{\sqrt{1-4\delta_n^2}} \cos \psi_n \\ \frac{-i\delta_n}{\sqrt{1-4\delta_n^2}} \sin \psi_n & \frac{-i\delta_n}{\sqrt{1-4\delta_n^2}} \cos \psi_n & \frac{-1+\sqrt{1-4\delta_n^2}}{2\sqrt{1-4\delta_n^2}} \end{pmatrix}, \quad (32)$$

where we have set

$$\lambda_1^{(n)} \equiv \frac{i}{2\lambda_\gamma^{(n)}(E_0)}, \quad \lambda_2^{(n)} \equiv \frac{i}{4\lambda_\gamma^{(n)}} \left(1 - \sqrt{1-4\delta_n^2}\right), \quad \lambda_3^{(n)} \equiv \frac{i}{4\lambda_\gamma^{(n)}} \left(1 + \sqrt{1-4\delta_n^2}\right) \quad (33)$$

with

$$E_n \equiv E_0 \left[1 + (n-1)\Delta z\right], \quad \delta_n \equiv \xi_n \lambda_\gamma^{(n)}(E_0) \left(\frac{\text{nG}}{10^{11} \text{ GeV}}\right), \quad (34)$$

where ξ_n is just ξ as defined by Eq. (20) and evaluated in the n -th domain.

E. Calculation of the photon survival probability in the presence of photon-ALP oscillations

Our aim is to derive the photon survival probability $P_{\gamma\gamma}^{\text{ALP}}(E_0, z)$ entering the text. So far, we have dealt with a single magnetic domain but now we enlarge our view so as to encompass the whole propagation process of the beam from the source to us. This goal is trivially achieved thanks to the analogy with non-relativistic quantum mechanics, according to which – for a fixed arbitrary choice of the angles $\{\psi_n\}_{1 \leq n \leq N_d}$ – the whole transfer matrix describing the propagation of the photon/ALP beam from the source at redshift z to us is

$$\mathcal{U}(E_0, z; \psi_1, \dots, \psi_{N_d}) = \prod_{n=1}^{N_d} \mathcal{U}_n(E_n, \psi_n) . \quad (35)$$

Moreover, the probability that a photon/ALP beam emitted by a blazar at z in the state ρ_1 will be detected in the state ρ_2 for the above choice of $\{\psi_n\}_{1 \leq n \leq N_d}$ is given by Eq. (14). Whence

$$P_{\rho_1 \rightarrow \rho_2}(E_0, z; \psi_1, \dots, \psi_{N_d}) = \text{Tr} \left(\rho_2 \mathcal{U}(E_0, z; \psi_1, \dots, \psi_{N_d}) \rho_1 \mathcal{U}^\dagger(E_0, z; \psi_1, \dots, \psi_{N_d}) \right) \quad (36)$$

with $\text{Tr} \rho_1 = \text{Tr} \rho_2 = 1$.

Since the actual values of the angles $\{\psi_n\}_{1 \leq n \leq N_d}$ are unknown, the best that we can do is to evaluate the probability entering Eq. (36) as averaged over all possible values of the considered angles, namely

$$P_{\rho_1 \rightarrow \rho_2}(E_0, z) = \left\langle P_{\rho_1 \rightarrow \rho_2}(E_0, z; \psi_1, \dots, \psi_{N_d}) \right\rangle_{\psi_1, \dots, \psi_{N_d}} , \quad (37)$$

indeed in accordance with the strategy outlined above. In practice, this is accomplished by evaluating the r.h.s. of Eq. (36) over a very large number of realizations of the propagation process (we take 5000 realizations) randomly choosing the values of all angles $\{\psi_n\}_{1 \leq n \leq N_d}$ for every realization, adding the results and dividing by the number of realizations.

Because the photon polarization cannot be measured at the considered energies, we have to sum the result over the two final polarization states

$$\rho_x = \begin{pmatrix} 1 & 0 & 0 \\ 0 & 0 & 0 \\ 0 & 0 & 0 \end{pmatrix} , \quad (38)$$

$$\rho_z = \begin{pmatrix} 0 & 0 & 0 \\ 0 & 1 & 0 \\ 0 & 0 & 0 \end{pmatrix} . \quad (39)$$

Moreover, we suppose here that the emitted beam consists 100% of unpolarized photons, so that the initial beam state is described by the density matrix

$$\rho_{\text{unpol}} = \frac{1}{2} \begin{pmatrix} 1 & 0 & 0 \\ 0 & 1 & 0 \\ 0 & 0 & 0 \end{pmatrix} . \quad (40)$$

We find in this way the photon survival probability $P_{\gamma\gamma}^{\text{ALP}}(E_0, z)$

$$\begin{aligned} P_{\gamma\gamma}^{\text{ALP}}(E_0, z) &= \left\langle P_{\rho_{\text{unpol}} \rightarrow \rho_x}(E_0, z; \psi_1, \dots, \psi_{N_d}) \right\rangle_{\psi_1, \dots, \psi_{N_d}} + \\ &+ \left\langle P_{\rho_{\text{unpol}} \rightarrow \rho_z}(E_0, z; \psi_1, \dots, \psi_{N_d}) \right\rangle_{\psi_1, \dots, \psi_{N_d}} , \end{aligned} \quad (41)$$

which is indeed the quantity entering Eq. (5) of the text.

A final remark is in order. It is obvious that the beam follows a single realization of the considered stochastic process at once, but since we do not know which one is actually selected the best we can do is to evaluate the average photon survival probability. Nevertheless, it can be shown that the considered realizations exhibit an oscillatory behavior for an energy close to the threshold E_L defined by Eq. (18). Therefore, observations performed at energies close enough to E_L should exhibit oscillations in the energy spectrum [65, 74]. This fact has been used to derive the previous bounds discussed in [72, 73].

-
- [1] <https://www.mpi-hd.mpg.de/hfm/HESS>
- [2] <https://magic.mpp.mpg.de/>
- [3] <http://veritas.sao.arizona.edu/>
- [4] <http://tevcat.uchicago.edu/>
- [5] For a review, see: E. Dwek, F. Krennrich, *Astroparticle Phys.* **43**, 112 (2013).
- [6] S. D. Bloom, A. P. Marscher, *Astrophys. J.* **461** 657 (1996).
- [7] F. Tavecchio, L. Maraschi, G. Ghisellini, *Astrophys. J.* **509** 608 (1998).
- [8] F. A. Aharonian, *Very High Energy Cosmic Gamma Radiation* (World Scientific, Singapore, 2004).
- [9] For a review, see: J. Jaeckel and A Ringwald, *Ann. Rev. Nucl. Part. Sci.* **60**, 405 (2010).
- [10] N. Turok, *Phys. Rev. Lett.* **76**, 1015 (1996).
- [11] E. Witten, *Phys. Lett. B* **149**, 351 (1984).
- [12] J. P. Conlon, *JHEP* **0605**, 078 (2006).
- [13] P. Svrcek and E. Witten, *JHEP* **0606**, 051 (2006).
- [14] J. P. Conlon, *Phys. Rev. Lett.* **97**, 261802 (2006).
- [15] K. -S. Choi, I. -W. Kim and J. E. Kim, *JHEP* **0703**, 116 (2007).
- [16] A. Arvanitaki et al., *Phys. Rev. D* **81**, 123530 (2010).
- [17] B. S. Acharya, K. Bobkov and P. Kumar, *JHEP* **1011**, 105 (2010).
- [18] M. Cicoli, M. Goodsell and A. Ringwald, *JHEP* **1210**, 146 (2012).
- [19] A. G. Dias, A. C. B. Machado, C. C. Nishi, A. Ringwald and P. Vaudrevange, *JHEP* **1406** 037 (2014).
- [20] P. Arias *et al.*, *JCAP*, **06** 008 (2012).
- [21] A. De Angelis, M. Roncadelli, O. Mansutti, *Phys. Rev. D* **76**, 121301 (2007).
- [22] A. Franceschini, G. Rodighiero, E. Vaccari, *Astron. Astrophys.* **487**, 837 (2008).
- [23] G. Breit, J. A. Wheeler, *Phys. Rev.* **46**, 1087 (1934).
- [24] W. Heitler, *The Quantum Theory of Radiation* (Oxford University Press, Oxford, 1960).
- [25] A. I. Nikishov, *Sov. Phys. JETP* **14**, 393 (1962).
- [26] R. J. Gould, G. P. Schröder, *Phys. Rev.* **155**, 1407 (1967).
- [27] G. G. Fazio, F. W. Stecker, *Nature* **226**, 135 (1970).
- [28] F. Tavecchio *et al.*, *Mon. Not. R. Astron. Soc.* **401**, 1570 (2010).
- [29] P. P. Kronberg, *Rept. Prog. Phys.* **57**, 325 (1994)
- [30] P. Blasi, S. Burles and A. V. Olinto, *Astrophys. J.* **514**, L79 (1999).
- [31] D. Grasso and H. R. Rubinstein, *Phys. Rep.* **348**, 163 (2001).
- [32] E. Massó and R. Toldra, *Phys. Rev. D* **52**, 1755 (1995).
- [33] J. W. Brockway, E. D. Carlson, G. G. Raffelt, *Phys. Lett. B* **383**, 439 (1996).
- [34] J. A. Grifols, E. Massó and R. Toldrá, *Phys. Rev. Lett.* **77**, 2372 (1996).
- [35] E. Massó and R. Toldra, *Phys. Rev. D* **55**, 7967 (1997).
- [36] S. M. Carroll, *Phys. Rev. Lett.* **81**, 3067 (1998).
- [37] C. Csáki, N. Kaloper and J. Terning, *Phys. Rev. Lett.* **88**, 161302 (2002).
- [38] C. Csáki, N. Kaloper and J. Terning, *Phys. Lett. B* **535**, 33 (2002).
- [39] M. Christensson and M. Fairbairn, *Phys. Lett. B* **565**, 10 (2003).
- [40] E. Zavattini *et al.*, *Phys. Rev. Lett.* **96**, 110406 (2006).
- [41] E. Zavattini *et al.*, *Phys. Rev. Lett.* **99**, 129901 (2007).
- [42] A. Dupays, C. Rizzo, M. Roncadelli and G. F. Bignami, *Phys. Rev. Lett.* **95**, 211302 (2005).
- [43] E. Massó and J. Redondo, *JCAP* **05**, 015 (2005).
- [44] C. Corianó and N. Irges, *Phys. Lett. B* **651**, 298 (2007).
- [45] M. Fairbairn, T. Rashba and S. Troitsky, *Phys. Rev. Lett.* **98**, 201801 (2007).
- [46] A. Mirizzi, G. G. Raffelt and P. D. Serpico, *Phys. Rev. D* **76**, 023001 (2007).
- [47] D. Hooper and P. D. Serpico, *Phys. Rev. Lett.* **99**, 231102 (2007).
- [48] K. A. Hochmuth and G. Sigl, *Phys. Rev. D* **76**, 123011 (2007).
- [49] A. De Angelis, O. Mansutti and M. Roncadelli, *Phys. Lett. B* **659**, 847 (2008).
- [50] M. Simet, D. Hooper and P. D. Serpico, *Phys. Rev. D* **77**, 063001 (2008).
- [51] A. De Angelis, O. Mansutti, M. Persic and M. Roncadelli, *Mon. Not. R. Astron. Soc.* **394**, L21 (2009).
- [52] A. Mirizzi and D. Montanino, *JCAP* **12** 004 (2009).
- [53] D. Chelouche, R. Rabadan, S. S. Pavlov and F. Castejon, *Astrophys. J. Suppl.* **180**, 1 (2009).

- [54] D. Chelouche and E. Guendelman, *Astrophys. J.* **699**, L5 (2009).
- [55] C. Burrage, A.-C. Davis and D. J. Shaw, *Phys. Rev. D* **79**, 044028 (2009).
- [56] M. A. Sánchez-Conde *et al.*, *Phys. Rev. D* **79**, 123511 (2009).
- [57] N. Bassan, A. Mirizzi and M. Roncadelli, *JCAP* **05** 010 (2010).
- [58] O. Mena, S. Razzaque and F. Villaescusa-Navarro, *JCAP* **02** 030 (2011).
- [59] A. Domínguez, M. A. Sánchez-Conde and F. Prada, *JCAP* **11** 020 (2011).
- [60] R. Gill and J. S. Heyl, *Phys. Rev. D* **84** 085001 (2011).
- [61] A. Payez, J. R. Cudell and D. Hutsemekers, *Phys. Rev. D* **84** 085029 (2011).
- [62] M. Fairbairn, T. Rashba and S. Troitsky, *Phys. Rev. D* **84** 125019 (2011).
- [63] D. Horns and M. Meyer, *JCAP* **02**, 033 (2012).
- [64] D. Horns, L. Maccione, A. Mirizzi and M. Roncadelli, *Phys. Rev. D* **85**, 085021 (2012).
- [65] D. Wouters, P. Brun, *Phys. Rev. D* **86** 043005 (2012).
- [66] D. Horns *et al.*, *Phys. Rev. D* **86**, 075024 (2012).
- [67] F. Tavecchio, M. Roncadelli, G. Galanti and G. Bonnoli, *Phys. Rev. D* **86**, 085036 (2012).
- [68] A. Friedland, M. Giannotti and M. Wise, *Phys. Rev. Lett.* **110**, 061101 (2013).
- [69] G. Carosi *et al.*, A snowmass white paper, arXiv:1309.7035.
- [70] J. P. Conlon and M. C. D. Marsh, *Phys. Rev. Lett.* **111**, 151301 (2013).
- [71] M. Meyer, D. Horns and M. Raue, *Phys. Rev. D* **87**, 035027 (2013).
- [72] A. Abramowski *et al.* [HESS Collaboration], *Phys. Rev. D* **88** 102003 (2013).
- [73] D. Wouters and P. Brun, *Astrophys. J.* **772**, 44 (2013).
- [74] G. Galanti, M. Roncadelli, arXiv:1305.2114.
- [75] M. Meyer and D. Horns, arXiv:1310.2058.
- [76] M. Meyer, D. Montanino and J. Conrad, *JCAP* **09**, 003 (2014).
- [77] S. Angus, J. P. Conlon, M. C. D. Marsh, A. Powell and L. T. Witkowski, *JCAP* **09** 026 (2014).
- [78] A. Ayala *et al.*, arXiv:1406.6053.
- [79] G. I. Rubtsov and S. V. Troitsky, *JETP Lett.* **100**, 355 (2014).
- [80] F. Tavecchio, G. Galanti and M. Roncadelli, arXiv:1406.2303.
- [81] D. Wouters and P. Brun, *JCAP*, **01** 016 (2014).
- [82] J. Harris, P. M. Chadwick, *JCAP* **10** 018 (2014).
- [83] M. Meyer and J. Conrad, *JCAP* **12**, 016 (2014).
- [84] A. Payez *et al.*, arXiv:1410.3747.
- [85] R. J. Protheroe and H. Meyer, *Phys. Lett. B* **493**, 1 (2000).
- [86] F. T. Aharonian *et al.* [H.E.S.S. Collaboration], *Nature* **440**, 1018 (2006).
- [87] T. M. Kneiske and H. Dole, *Astron. Astrophys.* **515**, 19 (2010).
- [88] J. Biteau and D. A. Williams, arXiv:1502.04166.
- [89] <https://www.cta-observatory.org/>.
- [90] <https://alps.desy.de/e141064>.
- [91] R. Bähre *et al.*, arXiv:1302.5647.
- [92] I. G. Irastorza *et al.* [IAEXO Collaboration], *JCAP* **06**, 013 (2011).
- [93] F. T. Avignone III, *Phys. Rev. D* **79**, 035015 (2009).
- [94] F. T. Avignone III, R. J. Crewick and S. Nussinov, *Phys. Lett. B* **681**, 122 (2009).
- [95] F. T. Avignone III, R. J. Crewick and S. Nussinov, *Astropart. Phys.* **34**, 640 (2011).
- [96] For a review, see: J. E. Kim and G. Carosi, *Rev. Mod. Phys.* **82**, 557 (2010).
- [97] S. L. Cheng, C. Q. Geng, and W. T. Ni, *Phys. Rev. D* **52**, 3132 (1995).
- [98] P. Sikivie, *Phys. Rev. Lett.* **51**, 1415 (1983); (E) *Phys. Rev. Lett.* **52**, 695 (1984).
- [99] G. G. Raffelt, L. Stodolsky, *Phys. Rev. D* **37**, 1237 (1988).
- [100] E. Arik *et al.* [CAST collaboration], *JCAP* **02**, 008 (2009).
- [101] S. R. Furlanetto and A. Loeb, *Astrophys. J.* **556**, 619 (2001).
- [102] S. Bertone, C. Vogt and T. Ensslin, *Mon. Not. R. Astron. Soc.* **370**, 319 (2006).
- [103] R. Durrer and A. Neronov, *Astron. Astrophys. Rev.* **21**, 62 (2013).
- [104] G. Hinshaw *et al.* [WMAP collaboration], *Astrophys. J. Suppl.* **180**, 225 (2009).
- [105] C. Csáki, N. Kaloper, M. Peloso, J. Terning, *JCAP* **05**, 005 (2003).

Source	z	Γ_{obs}	ΔE_0 [TeV]
3C 66B	0.0215	3.10 ± 0.37	0.12 – 1.8
Mrk 421	0.031	2.20 ± 0.22	0.13 – 2.7
Mrk 501	0.034	2.72 ± 0.18	0.21 – 2.5
1ES 2344+514	0.044	2.95 ± 0.23	0.17 – 4.0
Mrk 180	0.045	3.30 ± 0.73	0.18 – 1.3
1ES 1959+650	0.048	2.72 ± 0.24	0.19 – 1.5
1ES 1959+650	0.048	2.58 ± 0.27	0.19 – 2.4
AP LIB	0.049	2.50 ± 0.22	0.30 – 3.0
1ES 1727+502	0.055	2.70 ± 0.54	0.10 – 0.6
PKS 0548-322	0.069	2.86 ± 0.35	0.32 – 3.5
BL Lacertae	0.069	3.60 ± 0.43	0.15 – 0.7
PKS 2005-489	0.071	3.20 ± 0.19	0.32 – 3.3
RGB J0152+017	0.08	2.95 ± 0.41	0.32 – 3.0
1ES 1741+196	0.083	?	?
SHBL J001355.9-185406	0.095	3.40 ± 0.54	0.42 – 2.0
W Comae	0.102	3.81 ± 0.49	0.27 – 1.1
1ES 1312-423	0.105	2.85 ± 0.51	0.36 – 4.0
VER J0521+211	0.108	3.44 ± 0.36	0.22 – 1.1
PKS 2155-304	0.116	3.53 ± 0.12	0.21 – 4.1
B3 2247+381	0.1187	3.20 ± 0.71	0.15 – 0.84
RGB J0710+591	0.125	2.69 ± 0.33	0.37 – 3.4
H 1426+428	0.129	3.55 ± 0.49	0.28 – 0.43
1ES 1215+303	0.13	3.60 ± 0.50	0.30 – 0.85
1ES 1215+303	0.13	2.96 ± 0.21	0.095 – 1.3
RX J1136.5+6737	0.1342	?	?
1ES 0806+524	0.138	3.60 ± 1.04	0.32 – 0.63
1ES 0229+200	0.14	2.50 ± 0.21	0.58 – 11
1RXS J101015.9-311909	0.142639	3.08 ± 0.47	0.26 – 2.2
H 2356-309	0.165	3.09 ± 0.26	0.22 – 0.9
RX J0648.7+1516	0.179	4.40 ± 0.85	0.21 – 0.47
1ES 1218+304	0.182	3.08 ± 0.39	0.18 – 1.4
1ES 1101-232	0.186	2.94 ± 0.22	0.28 – 3.2
1ES 0347-121	0.188	3.10 ± 0.25	0.30 – 3.0
RBS 0413	0.19	3.18 ± 0.74	0.30 – 0.85
RBS 0723	0.198	?	?
1ES 1011+496	0.212	4.00 ± 0.54	0.16 – 0.6
MS 1221.8+2452	0.218	?	?
PKS 0301-243	0.2657	4.60 ± 0.73	0.25 – 0.52
1ES 0414+009	0.287	3.45 ± 0.32	0.18 – 1.1
S5 0716+714	0.31	3.45 ± 0.58	0.18 – 0.68
1ES 0502+675	0.341	3.92 ± 0.36	?
PKS 1510-089	0.361	5.40 ± 0.76	0.14 – 0.32
3C 66A	0.41	4.10 ± 0.72	0.23 – 0.47
PKS 1222+216	0.432	3.75 ± 0.34	0.08 – 0.36
1ES 0647+250	0.45	?	?
PG 1553+113	0.5	4.50 ± 0.32	0.23 – 1.1
3C 279	0.5362	4.10 ± 0.73	0.08 – 0.46
PKS 1424+240	≥ 0.6035	3.80 ± 0.58	0.14 – 0.5

TABLE III: Blazars observed at the time of writing above 100 GeV with the IACTs with known energy, redshift, spectral index Γ_{obs} and energy range. Statistical and systematic errors are added in quadrature to produce the total error reported on the measured spectral index. When only statistical errors are quoted, systematic errors are taken to be 0.1 for H.E.S.S., 0.15 for VERITAS, and 0.2 for MAGIC. Sources with question marks lack information to perform our analysis and are discarded. For PKS 1424+240 only a lower limit on the redshift exists in the literature: thus, it is neglected in our analysis.

Source	$\Gamma_{\text{em}}^{\text{CP}}$	$\Gamma_{\text{em}}^{\text{ALP}}$			
		$\xi = 0.1$	$\xi = 0.5$	$\xi = 1$	$\xi = 5$
3C 66B	3.00	3.00	3.00	3.01	3.03
Mrk 421	2.05	2.05	2.05	2.06	2.10
Mrk 501	2.54	2.54	2.54	2.55	2.59
1ES 2344+514	2.71	2.71	2.71	2.73	2.79
Mrk 180	3.07	3.07	3.07	3.09	3.14
1ES 1959+650	2.46	2.46	2.47	2.49	2.55
1ES 1959+650	2.32	2.32	2.32	2.35	2.40
AP LIB	2.21	2.21	2.22	2.24	2.31
1ES 1727+502	2.52	2.52	2.52	2.54	2.58
PKS 0548-322	2.44	2.44	2.45	2.51	2.58
BL Lacertae	3.29	3.29	3.30	3.33	3.39
PKS 2005-489	2.77	2.77	2.79	2.85	2.91
RGB J0152+017	2.47	2.47	2.48	2.56	2.63
1ES 1741+196	?	?	?	?	?
SHBL J001355.9-185406	2.81	2.81	2.84	2.94	3.01
W Comae	3.17	3.17	3.20	3.31	3.38
1ES 1312-423	2.17	2.17	2.21	2.34	2.40
VER J0521+211	2.79	2.79	2.82	2.93	3.00
PKS 2155-304	2.81	2.81	2.86	3.00	3.05
B3 2247+381	2.60	2.60	2.64	2.74	2.80
RGB J0710+591	1.89	1.89	1.96	2.12	2.16
H 1426+428	2.85	2.85	2.89	3.01	3.08
1ES 1215+303	2.75	2.75	2.81	2.97	3.03
1ES 1215+303	2.35	2.35	2.40	2.51	2.55
RX J1136.5+6737	?	?	?	?	?
1ES 0806+524	2.70	2.70	2.77	2.93	3.00
1ES 0229+200	0.61	0.62	1.20	1.43	1.26
1RXS J101015.9-311909	2.20	2.20	2.29	2.45	2.49
H 2356-309	2.05	2.05	2.17	2.35	2.40
RX J0648.7+1516	3.45	3.45	3.55	3.71	3.77
1ES 1218+304	1.97	1.97	2.13	2.31	2.34
1ES 1101-232	1.72	1.73	1.96	2.13	2.13
1ES 0347-121	1.87	1.87	2.11	2.28	2.28
RBS 0413	1.88	1.89	2.07	2.28	2.32
RBS 0723	?	?	?	?	?
1ES 1011+496	2.90	2.90	3.06	3.22	3.26
MS 1221.8+2452	?	?	?	?	?
PKS 0301-243	2.93	2.93	3.27	3.46	3.49
1ES 0414+009	1.65	1.65	2.12	2.26	2.25
S5 0716+714	1.60	1.61	2.07	2.22	2.22
1ES 0502+675	?	?	?	?	?
PKS 1510-089	4.02	4.02	4.33	4.45	4.48
3C 66A	1.53	1.54	2.31	2.40	2.39
PKS 1222+216	2.46	2.46	2.79	2.87	2.89
1ES 0647+250	?	?	?	?	?
PG 1553+113	0.98	1.09	2.52	2.30	2.16
3C 279	2.05	2.06	2.71	2.74	2.73
PKS 1424+240	≤ 0.44	≤ 0.50	≤ 1.66	≤ 1.61	≤ 1.56

TABLE IV: Blazars considered in the Table III. For each of them (first column), the deabsorbed value Γ_{em} is reported for different deabsorbing situations. The second column concerns deabsorption according to conventional physics, using the EBL model of FRV. The third column pertains the photon-ALP oscillation model with the EBL still described by the model of FRV, and report the values of Γ_{em} for different choices of the model parameter ξ and for $L_{\text{dom}} = 4 \text{ Mpc}$. The total error is the same as for Γ_{obs} and reported in the Table III (for more details see text). Sources with question marks lack information to perform our analysis and are discarded. For PKS 1424+240 only a lower limit for its z exists in the literature: thus, it is neglected in our analysis.

Source	$\Gamma_{\text{em}}^{\text{CP}}$	$\Gamma_{\text{em}}^{\text{ALP}}$			
		$\xi = 0.1$	$\xi = 0.5$	$\xi = 1$	$\xi = 5$
3C 66B	3.00	3.00	3.01	3.01	3.04
Mrk 421	2.05	2.05	2.05	2.07	2.10
Mrk 501	2.54	2.54	2.54	2.57	2.60
1ES 2344+514	2.71	2.71	2.72	2.76	2.79
Mrk 180	3.07	3.07	3.08	3.12	3.14
1ES 1959+650	2.46	2.46	2.48	2.52	2.55
1ES 1959+650	2.32	2.32	2.33	2.38	2.41
AP LIB	2.21	2.21	2.23	2.28	2.31
1ES 1727+502	2.52	2.52	2.53	2.56	2.58
PKS 0548-322	2.44	2.44	2.48	2.56	2.58
BL Lacertae	3.29	3.29	3.31	3.37	3.39
PKS 2005-489	2.77	2.77	2.82	2.89	2.92
RGB J0152+017	2.47	2.47	2.53	2.60	2.63
1ES 1741+196	?	?	?	?	?
SHBL J001355.9-185406	2.81	2.81	2.90	2.99	3.01
W Comae	3.17	3.17	3.27	3.36	3.38
1ES 1312-423	2.17	2.17	2.30	2.38	2.40
VER J0521+211	2.79	2.79	2.89	2.98	3.00
PKS 2155-304	2.81	2.81	2.95	3.03	3.05
B3 2247+381	2.60	2.60	2.71	2.78	2.80
RGB J0710+591	1.89	1.89	2.07	2.15	2.16
H 1426+428	2.85	2.85	2.97	3.06	3.08
1ES 1215+303	2.75	2.75	2.92	3.01	3.03
1ES 1215+303	2.35	2.35	2.47	2.54	2.56
RX J1136.5+6737	?	?	?	?	?
1ES 0806+524	2.70	2.71	2.88	2.98	3.00
1ES 0229+200	0.61	0.65	1.41	1.36	1.25
1RXS J101015.9-311909	2.20	2.20	2.41	2.48	2.49
H 2356-309	2.05	2.06	2.30	2.38	2.40
RX J0648.7+1516	3.45	3.45	3.67	3.75	3.77
1ES 1218+304	1.97	1.97	2.27	2.33	2.34
1ES 1101-232	1.72	1.73	2.10	2.14	2.13
1ES 0347-121	1.87	1.88	2.26	2.29	2.28
RBS 0413	1.88	1.89	2.24	2.31	2.32
RBS 0723	?	?	?	?	?
1ES 1011+496	2.90	2.90	3.19	3.25	3.26
MS 1221.8+2452	?	?	?	?	?
PKS 0301-243	2.93	2.94	3.43	3.48	3.49
1ES 0414+009	1.65	1.67	2.25	2.26	2.25
S5 0716+714	1.60	1.62	2.20	2.22	2.22
1ES 0502+675	?	?	?	?	?
PKS 1510-089	4.02	4.03	4.43	4.47	4.48
3C 66A	1.53	1.58	2.40	2.39	2.39
PKS 1222+216	2.46	2.48	2.86	2.88	2.89
1ES 0647+250	?	?	?	?	?
PG 1553+113	0.98	1.42	2.38	2.22	2.16
3C 279	2.05	2.13	2.74	2.74	2.73
PKS 1424+240	≤ 0.44	≤ 0.70	≤ 1.63	≤ 1.58	≤ 1.56

TABLE V: Same as Table IV, but with $L_{\text{dom}} = 10$ Mpc.